A nine-year record of slush on the Greenland Ice Sheet

Emily Glen[1,2,3], Alison F. ~~Banwell[3,4]~~Banwell[4,5], Katie E. Miles[1], Amber A. Leeson[1,2], Rebecca L. ~~Dell[5]~~Dell[6], Malcolm McMillan[1,2], Jennifer Maddalena[1,2]

[1] Lancaster Environment Centre, Lancaster University, Lancaster, UK
[2] Centre for Polar Observation and Modelling, Lancaster University, Lancaster, UK
~~[3]~~[3] Department of Geography, Pennsylvania State University, University Park, PA, USA
[4] Cooperative Institute for Research in Environmental Sciences (CIRES), University of Colorado Boulder, Boulder, USA
~~[4] Centre~~[5]Centre for Polar Observation and Modelling, School of Geography and Natural Sciences, Northumbria University, Newcastle Upon Tyne, UK
~~[5]~~[6] Scott Polar Research Institute, University of Cambridge, Lensfield Road, Cambridge, UK

Correspondence to: Emily Glen (~~e.~~emily_glen@~~lancaster.ac.uk~~psu.edu)

Abstract. Surface melt on the Greenland Ice Sheet (GrIS) has intensified in recent decades, accelerating ~~GrIS~~ice sheet mass loss. Slush (i.e~~.,~~., water-saturated firn or snow) is a key component of this system, yet its areal extent and behaviour ~~remains~~remain poorly constrained. Here, we present the first GrIS-wide classification of slush~~,~~ using ~~over 300,000~~ Sentinel-2 ~~images~~imagery and a supervised Random Forest classifier implemented in Google Earth Engine~~. We generate~~, generating a nine-year (2016~~–~~-2024~~), high spatial resolution (10 m~~) dataset~~, which we then use~~ used to perform ~~an~~the first ice~~-~~-sheet~~-~~-wide systematic assessment of slush distribution across all ~~six major~~GrIS drainage basins. On average, slush covers ~2.9% ~~(~~~(50,~~400~~300-51,055 km²) of the ~~entire~~ GrIS each summer, with ~~around 40% (~~~maximum seasonal extents ranging from ~1.2% (20,460-20,770 km²) in 2018 to ~5.2% (90,120-91,470 km²) in 2019. Slush is most extensive in the southwestern and northern basins, most persistent in the northeast and north, and maximum slush elevation co-varies with areal extent across all basins. Over the nine-year record, ~71% of all mapped slush occurs over the bare ice zone and ~29~~,300 km²) of this area in regions with low-permeability ice~~% within the firn zone. Notably, ~30% of total slush co-occurs with ice slab extents, a proportion increasing with persistence, consistent with slabs ~~or by firn aquifers. Slush shows marked~~acting as semi-permeable barriers favouring recurrent slush formation, while a further ~15% occurs within the firn zone outside mapped slab extents, suggesting smaller-scale firn heterogeneity may locally impede vertical meltwater infiltration. Interannual variability ~~that mirrors variability in~~in slush extent is most strongly associated with firn air content, followed by snowmelt and air temperature; at intra-annual timescales, monthly slush extent is most strongly associated with concurrent and antecedent snowmelt. Extreme melt ~~intensity, ranging from a maximum slush areal extent of 1.2% (20,500 km²) of the ice sheet in 2018, the lowest~~years may also precondition the ice sheet for enhanced slush recurrence in subsequent seasons, as suggested by persistently elevated slush extent in the northern basin following 2019, even during years of modest melt~~ year of the time series, to a maximum of 5.2% (90,300 km²) in 2019, the highest melt year. When our results are evaluated alongside those from other studies, we find that~~. Slush is the dominant surface meltwater feature on the GrIS in terms of spatial coverage~~ on the GrIS each melt season: the~~:

maximum slush area was nine and four times greater than the combined area of supraglacial lakes and ~~streams~~channels in 2019 and 2018, respectively. ~~As climate change drives more frequent and prolonged extreme melt seasons on the GrIS, slush is~~ Continued warming and declining firn retention capacity are likely to ~~increase in area. Given the influence of slush on lateral meltwater transport, firn-air depletion, and melt–albedo feedback, its incorporation into~~favour more extensive and persistent slush formation, and explicit representation of slush in surface energy balance and hydrological models ~~will help~~is required to better constrain future ice~~-~~ sheet mass~~-~~-balance projections.

1. Introduction

The Greenland Ice Sheet (GrIS) has experienced a negative mass balance for several decades, losing ice at a rate of ~~=~~255 ± 19 Gt yr^{-1} from 2002 to 2022 (Otosaka et al., 2023). Supraglacial melting and runoff are ~~the principal~~major drivers of this mass loss, accounting for ~~~70%~~just over half of total ice sheet mass loss between ~~2007 – 2012~~1992 and 2018 (IMBIE, 2020). ~~Between 1991–2019, the~~ Mean summer air temperature on the GrIS has increased by ~1.7°C from 1991 to 2019 (Hanna et al., 2021), contributing to a 21% increase in supraglacial runoff between 2011 and 2020 compared to the previous three decades (Slater et al., 2021; Trusel et al., 2018). Superimposed on this long-term warming trend are increasingly frequent extreme melt events (Bonsoms et al., 2024); short-lived episodes of anomalously intense melting typically driven by persistent high-pressure systems (Tedesco and Fettweis, 2020). In response to both long-term warming and an increase in the frequency of extreme melt events, supraglacial meltwater features, particularly lakes, have expanded in both area and elevation over recent decades (Fan et al., 2025; Leeson et al., 2015; Howat et al., 2013), with the maximum elevation of runoff shifting inland by up to 329 m a.s.l. in elevation between 1985 and 2020 (Tedstone and Machguth, 2022). In some regions, melt now ~~reaches far~~extends further inland into the percolation zone, ~~areas~~an area that has historically experienced little or no seasonal melting (Tedesco, 2007; Fettweis et al., 2011~~), creating~~). Enhanced meltwater production, together with reductions in firn storage capacity, can create conditions favourable for the formation of slush, ~~which we define~~defined here as fully water-saturated firn or snow (Cogley et al., 2011).

Slush, first observed during~~ early~~ Greenland expeditions in the early twentieth century and formally described by Holmes (1955), typically forms in the percolation zone when vertical drainage is impeded, either by a low~~-~~-permeability ice layer or by saturation of the firn pore space, which waterlogs the overlying firn and snow. Holmes (1955) distinguished between surface slush and ~~subsurface~~sub-surface slush. Surface slush is fully saturated at the surface and can be detected in optical satellite imagery (referred to as blue slush), whereas sub-surface slush is overlain by ~~an~~ unsaturated snow (referred to as white slush) and therefore cannot be identified in optical imagery (Greuell and Knap, 2000; Machguth et al., 2022~~.~~). Once slush forms, the reduced vertical permeability causes meltwater to be preferentially routed laterally. This process enhances surface hydrological connectivity, as meltwater flows more readily through slush than through dry snow and firn (Clerx et al., 2022), feeding supraglacial ~~rivers~~channels and lakes (Holmes, 1955). Slush can act as a precursor to supraglacial channelisation, either through directing excess meltwater into topographic depressions where channel incision is initiated (Chu, 2014; Rippin and

Rawlins, 2021), or through removal of the previous winter's snow from an existing channel (Tedesco et al., 2013). These channels can link to moulins or crevasses, providing a pathway through which meltwater can be routed to the ice~~-~~ sheet bed (Tedesco et al., 2013; Banwell et al., 2013~~;~~, 2016) thereby ~~promoting~~influencing basal lubrication and ~~dynamic~~ ice ~~loss~~dynamics (e.g., de Fleurian et al., 2018; Koziol and Arnold 2018). Upon refreezing, slush has the potential to create new and thicken pre-existing near-surface ice slabs (Tedstone et al., 2025). These multi-metre-thick bodies of refrozen ice can extend over tens of kilometres (Machguth et al., 2016; MacFerrin et al., 2019; Jullien et al., 2025) and, due to their low permeability, restrict vertical meltwater transport and storage, enhancing runoff from inland areas (Machguth et al., 2016; Tedstone and Machguth, 2022; Culberg et al., 2024).

Despite its hydrological importance, slush remains largely absent from large-scale meltwater mapping efforts across the GrIS. Only a limited number of studies have attempted to quantify the areal extent and/or elevation of slush, either through catchment-scale mapping of its spatial distribution (e.g., Covi et al., 2022; Rawlins et al., 2023; Glen et al., 2025) or~~–~~, at larger spatial scales~~–~~, by identifying the 'runoff limit', defined as the highest elevation where visibly saturated firn or snow is present in satellite imagery (~~Gruell~~Greuell and Knap, 2000; Tedstone and Machguth, 2022; Machguth et al., ~~2023~~2022). Recent observations suggest that both the elevation and areal extent of slush are highly sensitive to interannual melt variability. For example, within the Watson catchment, southwest Greenland, slush was found to cover a substantially larger area and extend to higher elevations during the extreme melt year of 2019 compared to the below-average melt year of 2018~~,~~ ~~(Glen et al., 2025),~~ increasing from ~1.6% of the catchment (~80 km^2) in 2018 to 7.6% ~~(~~(~380 km^2) in 2019, and expanding upslope from elevations below 1,500 m a.s.l. to above 1,800 m a.s.l. (Glen et al., ~~.~~2025). Similarly, long-term satellite analyses indicate a systematic upward migration of the runoff limit of the GrIS, with Landsat imagery revealing a 29% ~~increase~~expansion in ~~elevation~~runoff area between 1985 and 2020 (Tedstone and Machguth, 2022), and MODIS imagery detecting slush at elevations approaching ~2080 m a.s.l. in western Greenland (Machguth et al., ~~2023).~~ 2022).

Recent findings from Antarctic ice shelves further emphasise the importance of slush within polar ice sheet hydrological and mass balance systems more generally. Dell et al. (2024) show that, in January (mid-austral summer), slush accounts for approximately 50% of the total meltwater area across 57 ice shelves, suggesting that previous meltwater inventories~~—focused~~, which focus primarily on supraglacial lakes and channels~~—~~, significantly underestimate total meltwater ~~storage in Antarctica. Given the climatological similarities between Antarctic ice shelves and the percolation zone of the GrIS, it is reasonable to hypothesize that similar findings may apply to Greenland as well.~~area. Dell et al. (2024) demonstrate that incorporating ~~slush~~ surface meltwater processes (including slush and ponded water) into regional climate models ~~—especially~~ via the ~~positive~~ melt-albedo feedback from surface saturation (e.g. Banwell et al., 2023) ~~—~~nearly triples ~~modeled~~modelled snowmelt. Fully accounting for slush in ice sheet meltwater budgets and climate models is therefore crucial to better estimate surface melt and runoff, both now and into the future.

Here, we adapt a machine learning (ML) workflow developed for Antarctic ice shelves (Dell et al., 2022~~;~~, 2024) to classify blue surface slush (henceforth *'slush'*) across the entire GrIS using Sentinel-2 imagery in Google Earth Engine (GEE). This represents the first application of ML to map slush on the GrIS, through which we generate an ice-sheet-wide dataset of slush extent spanning nine years (2016~~–~~-2024). Using these data, we ~~analyse spatial and temporal patterns across all six major drainage basins, and~~ characterise the ice-sheet-wide distribution~~, interannual~~ of slush across all six major drainage basins, examining its spatial and temporal variability, elevation patterns, potential controls, and ~~the~~ relative importance ~~of slush~~ within the ~~GrIS'~~ broader GrIS meltwater regime.

2. Methods and data

To date, the majority of remote sensing studies of ice sheet surface meltwater have focused on supraglacial lakes and channels, which are meltwater features with relatively distinct spectral characteristics and well-defined boundaries. Therefore, compared to slush, these features can be mapped with reasonable accuracy using threshold-based methods, such as the Normalised Difference Water Index adapted for ice ($NDWI_{ice}$) (e.g., Williamson et al., 2017, 2018; Miles et al., 2017). Slush has diffuse boundaries and a muted blue hue in optical imagery, making it difficult to isolate using standard thresholding techniques. In such approaches, slush is typically either omitted entirely (classified as 'non-water') or included within broader 'water' classes without being distinguished from lakes or channels, leading to underestimation or mischaracterisation of its extent (e.g., Rawlins et al., 2023; Yang and Smith, 2012).

Random Forest (RF) algorithms (e.g., Dirscherl et al., 2020; Dell et al., 2022~~;~~, 2024) and deep learning methods (e.g., Qayyum et al., 2020; Dunmire et al., 2025) have recently shown promise as an alternative to image thresholding for meltwater classification in both Greenland and Antarctica. For slush specifically, Dell et al. (2022, 2024~~),~~) employed a k-means clustering approach to generate training classes from Landsat 8 imagery, which were then used to train an RF classifier to identify slush (and supraglacial water bodies) on Antarctic ice shelves. However, no study has yet applied ML classification methods such as these specifically for slush detection on the GrIS.

Here, we ~~classify~~classified slush on the GrIS by following the approach outlined by Dell et al. (2022, 2024), but with adaptations for application to the GrIS, as detailed in the following sections and Figure 1. ~~We conduct~~We retained the general workflow of Dell et al. (2022, 2024), who originally applied it to Landsat 8 optical imagery, including k-means clustering for training data generation, $NDWI_{ice}$-based pre-thresholding, and RF classification in GEE. However, we made several adaptations for application to Sentinel-2 (S2) imagery, including specifically adjusted spectral thresholds to reflect sensor differences, and the addition of RF hyperparameter optimisation to improve classification performance. All image pre-processing, training data generation, RF classification, and post-processing were implemented in GEE, with final binary slush masks exported at 100 m spatial resolution (Glen et al., 2026). We conducted our analysis across all six basins of the GrIS:

Southwest (SW), Central West (CW), Northwest (NW), North (NO), Northeast (NE) and Southeast (SE) (Fig. 2; Mouginot and Rignot, 2019).

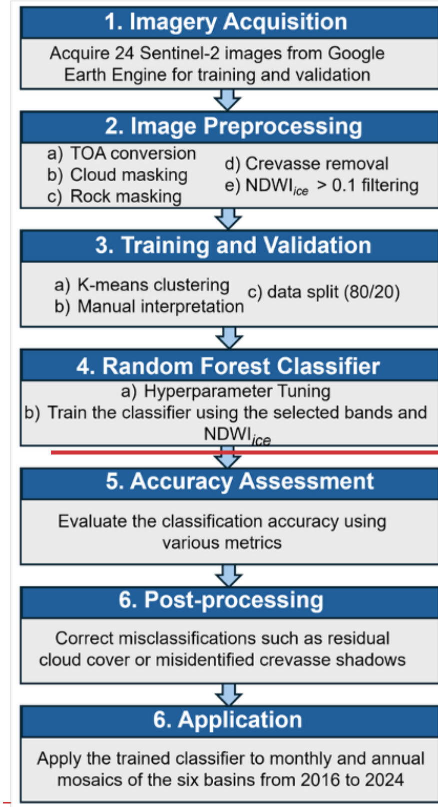

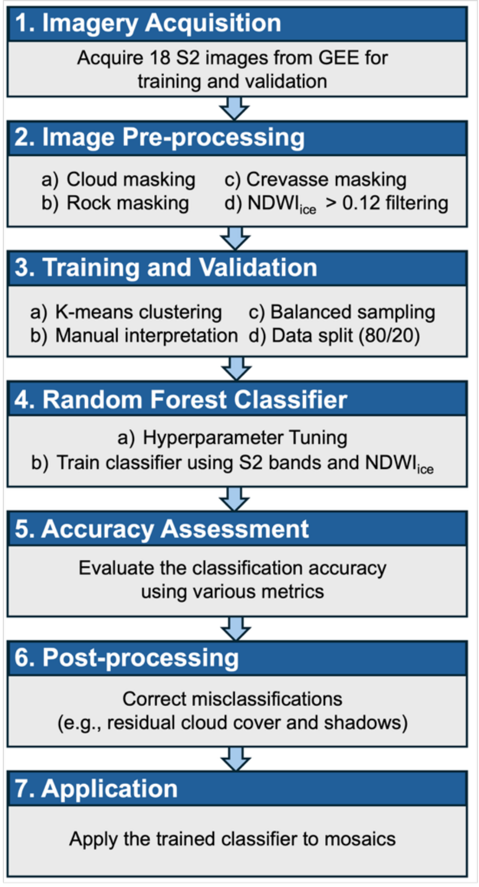

Figure 1: Flowchart of slush classification methodology adapted from Dell et al. (2022, 2024; Antarctic ice shelves) for application to the GrIS in this study.

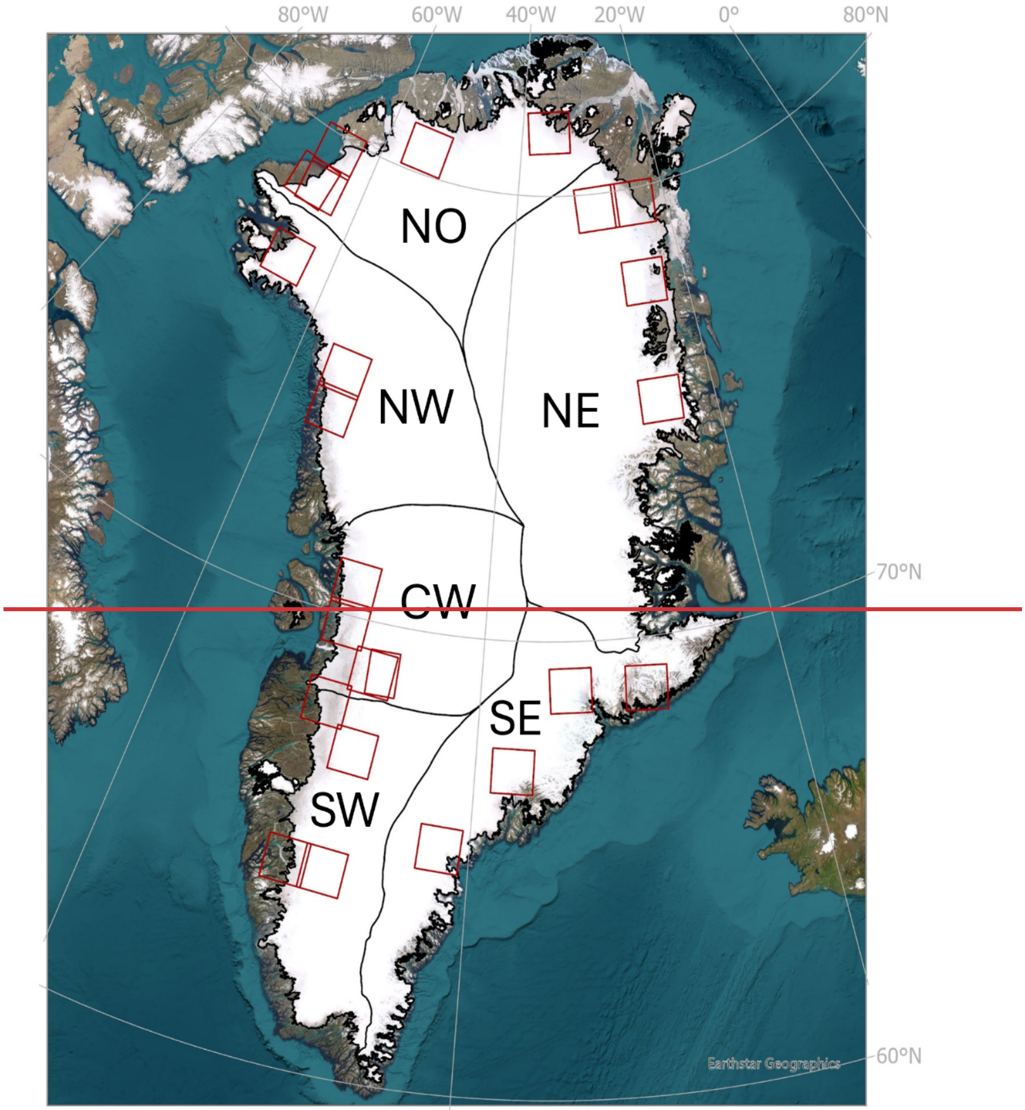
80°W
60°W
40°W
20°W
0°
80°N
70°N
60°N
NO
NW
NE
CW
SE
SW
Earthstar Geographics

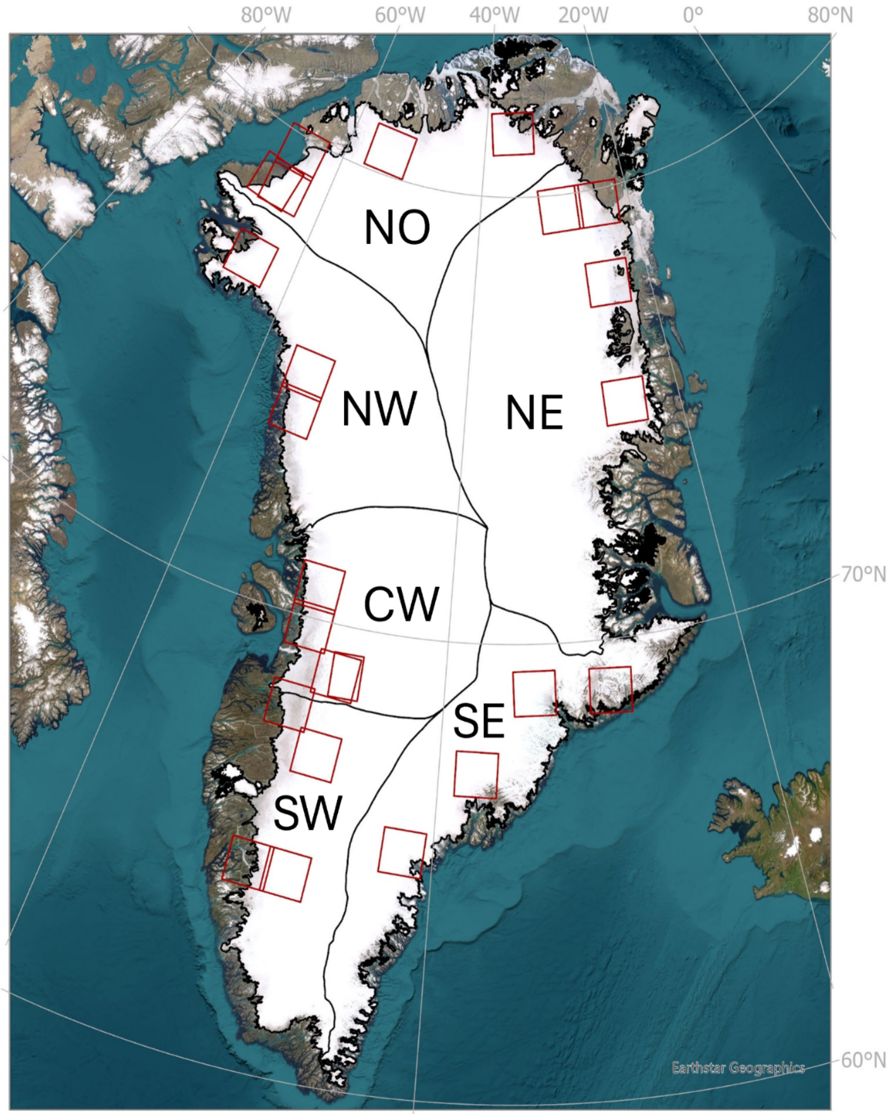

Figure 2: Overview map of the GrIS separated into six drainage basins: SW, CW, NW, NO, NE and SE (Mouginot and Rignot, 2019). Red boxes indicate footprints of the 24 S2 images used in this study: 18 for training~~/~~ and validation ~~images used to train and validate~~of the RF classifier, and a further 6 used ~~in this study~~for comparison against threshold-based classification methods. Base map source: Esri.

2.1. Data

2.1.1. Sentinel-2 imagery

We acquired and pre-processed Level-1C ~~Sentinel-2 (~~S2~~)~~ MultiSpectral Instrument (MSI) imagery from the European Space Agency (ESA) via the GEE data catalogue, processing a total of 329,229 images from May to September, 2016 to 2024. ~~Images were converted to ~~As Level-1C imagery is already provided as top-of-atmosphere reflectance~~ using a scaling factor of~~, pixel values were divided by 10,000 to scale reflectance values between 0 and 1 (ESA, 2015). To improve meltwater feature detection, we restricted the dataset to scenes with a solar elevation angle > 20° (Halberstadt et al., 2020) and cloud cover < 25~~%. All available MSI bands were used in the analysis.~~%, following common filtering approaches used in supraglacial meltwater mapping studies (e.g., Corr et al., 2022; Glen et al., 2025; Tuckett et al., 2025). Although pixel-level cloud masking was applied subsequently, this pre-filter helped reduce residual cloud-shadow artefacts and ensured sufficient clear-sky pixel coverage for compositing. All available MSI bands were used in the analysis.

2.1.2. Supporting datasets

We used the 2 m ArcticDEM mosaic (Porter et al., 2023) to provide high-resolution surface topography across the ice sheet. The ArcticDEM ~~is~~was used to mask crevassed areas following Chudley et al. (~~2020~~2021) as well as to determine the maximum elevation of slush reached during the melt season. For the latter, ArcticDEM elevations were sampled every 500 m along the upper limit of mapped slush across the ice sheet and averaged to estimate the maximum slush elevation.

Firn extent from 2000 to 2017 was taken from Vandecrux et al. (2019), based on firn density observations and end-of-summer snowline data. Ice slab extents were taken from Jullien et al. (2023), who used airborne accumulation radar data collected across the ~~Greenland Ice Sheet~~GrIS between 2002 and 2018 to map spatial variations in ice slab extent and thickness. We use both their ~~“high-end”~~'low-end' and 'high-end' estimates of slab extent in our analysis. Firn aquifer extents were taken from Miège et al. (2016), who identified ~~widespread ~~aquifers using ~~NASA~~NASA’s Operation IceBridge accumulation radar flown during five airborne campaigns between 2010 and 2014.

~~Melt~~Snowfall, melt, and air temperature data were obtained from the Regional Atmospheric Climate Model RACMO2.3p2 (hereafter ‘RACMO’; Noël et al., 2019). RACMO is forced by ERA5 and provides monthly snowfall, surface melt and 2 m air temperature ~~and surface melt ~~fields at 5.5 km spatial resolution, statistically downscaled to 1 km (Noël et al., 2018, 2019). ~~Melt and ~~Firn air content (FAC) was derived from the Institute for Marine and Atmospheric Research - Firn Densification Model (IMAU-FDM), a one-dimensional semi-empirical model also forced by ERA5 and dynamically downscaled using RACMO, which provides FAC fields at 10-day temporal and 5.5 km spatial resolution (Brils et al., 2022).

Snowfall, melt, air temperature and FAC anomalies were calculated relative to the ~~1958–2015~~1960-1989 monthly climatology, a period during which the ice sheet is assumed to have been approximately in steady state with climate forcing (Smith et al., 2020). Anomalies were calculated for each summer month (May~~–~~–September) and for each year between 2016 and 2024. These anomaly datasets were used to characterise interannual variability in snowfall, melt~~ and near-surface~~, air temperature and FAC during our study period.

2.2 Image pre-processing

2.2.~~2~~1. Image masking

To mask confounding surface features, we applied a cloud-detection algorithm based on S2-specific thresholds from Glen et al. (2025), following Corr et al. (2022), ~~adding~~with a 1 km buffer to account for cloud shadows. Rock outcrops were excluded using a modified Normalised Difference Snow Index ~~(NDSI;~~approach as detailed in Glen et al. (2025), following Moussavi et al~~.,~~. (2020), also buffered by 1 km to ensure complete removal. A crevasse mask, derived from 2 m ArcticDEM data (Porter et al., 2023), was used to remove crevasses to prevent misclassification errors (Chudley et al., 2021).

Meltwater features, including slush, were then isolated using an NDWI_{ice} (equation 1) threshold, which is a variant of the ~~'~~standard ~~NDWI'~~NDWI (McFeeters, 1996). While the standard NDWI, calculated from the green (B3) and near-infrared (B8) bands, is best for terrestrial environments and, in some cases, ice sheet surfaces (e.g. Box and Ski, 2007), NDWI_{ice} is specifically optimised for ice and firn surfaces and instead uses the blue (B2) and red (B4) bands (Yang and Smith, 2012).

$$NDWI_{Ice} = \frac{B2-B4}{B2+B4} \qquad (1)$$

While Dell et al. (2022) applied a > 0.1 NDWI_{ice} threshold for Antarctic ice shelves, we increased this to > 0.12 for Greenland (Yang and Smith, 2012) to account for regional differences in surface albedo and reflectance. Additionally, we used a blue band reflectance threshold of > 0.03 to filter out shadows cast by rocks, crevasses, and other non-meltwater features (Dirscherl et al., 2020; Corr et al., 2022).

2.2.~~3.~~2. S2 image mosaic creation

Monthly and annual S2 mosaics were generated for each basin over the period 2016~~–~~–2024 (May~~–~~–September). After image filtering and masking, all available S2 images were combined into mosaics using the *qualityMosaic* function in GEE, which retains the maximum NDWI_{ice} value for each pixel across overlapping images to capture the strongest meltwater signal in a given month or year (Dell et al., 2022). These monthly and annual mosaics were then used as the input datasets for the RF classifier (Section 2.4~~)~~).

2.3. Label generation for model training and validation

For each GrIS drainage basin (Fig. 2), we manually selected four S2 images (~~24~~18 images in total across all basins) for training and validation (Table S1). Images were chosen from the 2016~~–~~-2024 melt seasons (1 May to 30 September) and selected to capture spectral variability by representing a range of solar elevation angles (42~~°–~~°-75°) and both high- and low-melt conditions. All images were clipped to the boundaries of the six drainage basins (Fig. 2).

Following pre-processing, residual non-meltwater elements such as faint cloud shadows and crevasse artefacts were manually removed through visual inspection to ensure only meltwater features were retained for analysis. Although the proportion of features requiring manual correction could not be fully quantified, such instances were infrequent and typically limited to small, spectrally ambiguous areas in regions with complex topography.

Training and validation data were derived from the ~~24~~18 pre-processed S2 images using k-means clustering, following the approach of Halberstadt et al. (2020) and Dell et al. (2022). This method combines automated clustering with ~~manual~~expert interpretation, ~~which~~allowing large volumes of training data to be generated while avoiding time-intensive pixel-level manual labelling. By grouping pixels with similar spectral characteristics, the clustering approach can also reveal spectral patterns that may be overlooked ~~in~~through manual ~~labelling~~interpretation alone. The k-means algorithm grouped pixels ~~based on spectral characteristics~~ using all S2 bands ~~as well as the~~ and $NDWI_{ice}$. For each image, 100,000 pixels were sampled and 5 to 70 clusters were generated (Dell et al., 2022).

Clusters were manually reviewed by a single expert analyst, consistent with Dell et al. (2022), and assigned to ~~identify 'slush,' defined~~either 'slush' or 'non-slush' classes. Slush was identified as dense, light~~-~~-blue ~~patches~~areas in true-colour S2 image composites, ~~versus~~while the 'non-~~slush,' which~~slush' class included all other surface types (e.g., supraglacial lakes, channels, shadows, sediment, cryoconite), with any residual masked surfaces (e.g., rock, cloud, crevasses) also incorporated~~ into the 'non-slush' class.~~. Clusters that could not be confidently assigned to either class were excluded. ~~From the remaining clusters,~~ An equal number of pixels (2,000 per class) were randomly selected from the interpreted clusters to create a balanced dataset, which was then randomly split into 80% for model training and a withheld 20% for validation. We acknowledge that the distinction between slush and ponded water is not always sharply defined and therefore contains an element of expert judgement; illustrative examples used to guide interpretation are provided in the Supplement (Fig. S1). The final cluster assignments for all training images are provided in Table S2.

2.4. RF model training and validation

Following Dell et al (2022), the classification of slush from S2 satellite imagery was performed using a RF classifier, implemented within GEE (*ee.Classifier.smileRandomForest*). This is an ensemble learning method that trains multiple decision trees on random subsets of data and features and classifies by majority voting (Breiman, 2001). In this study, the RF classifier was applied to all S2 bands as well as the NDWI$_{ice}$ band~~ (Dell et al., 2022). ~~.

Unlike Dell et al. (2022), who used default settings, we optimised RF hyperparameters through an iterative tuning approach, systematically varying one parameter at a time and evaluating validation accuracy across each parameter range (Fig. S2). Parameters tested included the number of trees, bag fraction, minimum leaf population~~,~~ and maximum nodes~~, and random seed~~. Validation accuracies were compared across configurations, and the optimal setup was selected based on the highest observed accuracy. The final model used 50 trees, a bag fraction of 0.7, and a minimum leaf population of 20, with full details provided in Table ~~S2~~S3.

2.4.1. Model performance

We evaluated ~~**performance of the**~~ RF classifier performance using the withheld 20~~ ~~% validation dataset (Fig. S3; Table ~~**S3). Confusion matrices provided**~~S4). Performance was assessed using overall accuracy, ~~**the**~~Cohen's Kappa statistic (κ), ~~**F1-scores,**~~ precision, ~~**and**~~ recall~~**. Commission errors occur when non-slush**~~, and the F1-score. Overall accuracy represents the proportion of all validation pixels ~~**are incorrectly**~~ classified correctly, while κ quantifies agreement between predicted and observed classes beyond that expected by chance. Precision describes the proportion of pixels classified as slush that were truly slush, thereby reflecting commission error (false positives), ~~**while omission errors occur when**~~ whereas recall describes the proportion of true slush pixels ~~**are missed**~~successfully identified by the classifier and therefore reflects omission error (false negatives). The F1-score provides the harmonic mean of precision and recall, offering a balanced measure of classifier skill for each class.

The classifier achieved high overall performance (overall accuracy = 97.5%, κ = 0.85~~), with strong F1-scores for both~~). For the slush ~~(~~class, precision was 98.7%, recall was 98.5%, and the resulting F1-score was 98.6~~%) and~~ %, indicating both low commission and omission error. For the non-slush ~~(~~class, precision was 84.5%, recall was 88.4%, and the F1-score was 86.4~~%).~~%. In terms of ~~the number of misclassified pixels~~absolute pixel counts, 1,133 non-slush pixels were incorrectly labelled as slush ~~and~~ (false positives), while 1,000 slush pixels ~~labelled~~were classified as non-slush~~,~~ (false negatives), indicating a slight tendency ~~of~~for the RF classifier to overpredict slush (Fig. ~~S3).~~

S3). Based on these values, mapped slush area has an estimated uncertainty of +1.3% and -0.2% of the total slush area; these uncertainty bounds will be presented alongside our results from here on.

2.5. Application of trained RF model

Once trained, the supervised RF classifier was applied across all six drainage basins (Fig. 2) to the monthly and annual S2 image mosaics acquired between 2016 and 2024 (Section 2.1.3).

As in previous studies (e.g., Corr et al., 2022), manual post-processing was carried out to correct obvious misclassifications, including removal of areas of residual cloud cover and shaded areas near crevasses and fjords. Approximately 5~~–~~-7% of pixels in each final mosaic were identified as misclassified and removed from the dataset. Our mosaicing approach ensured consistent monthly coverage across the record, and no year was disproportionately affected by cloud or temporal gaps~~. This strengthens confidence that~~ (Fig S4), minimising the ~~enhanced slush extents observed in high-melt years, for example, reflect genuine surface conditions rather than artefacts~~potential influence of ~~reduced~~variable image availability and cloud cover on observed interannual differences (e.g., Hofer et al., 2017).

2.6. Comparison of the trained RF model to thresholding methods

We compared a subset of our RF slush classification results to those using two threshold-based methods: an NDWI approach combining both the standard NDWI and the $NDWI_{ice}$ (Glen et al., 2025) and a Greenness Index (G_{ind}; Covi et al., 2022). ~~Across test regions (i.e.~~For this comparison, one S2 image per basin ~~over~~was selected from across the nine~~ years),~~-year record (six test images in total). RF showed stronger agreement with NDWI than with G_{ind}, with higher overlap areas and F1-scores (0.56~~–~~-0.76 vs. 0.53~~–~~-0.65). Visual inspection confirmed these trends: NDWI aligned well with RF but was more prone to cloud contamination, while G_{ind} often underdetected slush and misclassified lake edges. RF consistently produced more spatially coherent outputs, particularly when complex surface types with high variability in spectral characteristics were present. Full details of this analysis, including evaluation metrics, visual examples and details regarding the limitations of our classifier, are presented in the Supplement (Section S1-S2; Fig. ~~S1~~S5; Table S5-S6).

3. Results

3.1. Mean spatial distribution and persistence of slush from 2016-2024

Between 2016 and 2024, slush was detected across all six drainage basins of the GrIS (Fig. 3), with a mean summer (May~~–~~-September) areal extent of ~2.9% ~~(50,400 km²)~~ of the ice sheet~~.~~, equivalent to 50,400 km², with a range of 50,300-51,055 km², accounting for uncertainty. Here and elsewhere, this range reflects an asymmetric uncertainty of +1.3%/-0.2% relative to the reported slush area (see Section 2.4.1). The highest concentrations of slush typically occurred 10~~–~~-20 km inland (Fig. 3), but slush was observed as far as 170 km inland during the most extreme melt year; 2019 (Fig. 4c).

Although slush was observed in every basin, its spatial coverage varied across the ice sheet (Fig. 3). Between 2016 and 2024, the SW basin exhibited the greatest proportional coverage (11,~~550~~530-11,700 km²; ~ 5.5% of ~~its~~ basin area), followed by the NO basin (11,~~660~~640-11,810 km²; ~ 4.8%), NE basin (14,~~590~~560-14,780 km²; ~ 3.0%), CW basin (4,~~430~~420-4,490 km²; ~ 1.9%), and NW basin (5,~~010~~000-5,080 km²; ~ 1.8%). The SE basin showed the lowest ~~areal~~slush extent ~~of slush~~ (1,730-1,750 km²; ~ 0.6%).

Slush persistence, defined as the number of melt seasons in which slush was detected at a given location, was examined on an interannual basis. Mean persistence was found to be highest in the NE and NO basins, where slush reappeared in the same locations during four out of nine melt seasons, whereas mean slush persistence was moderate in the NW and SW basins (three years) and lowest in the CW and SE basins (two years) (Fig. 3).

~~Considering~~ The area of slush across the ice sheet as a whole~~, slush-covered~~ reached as much as 149,~~660~~360-151,610 km^2 (~9% of the ice sheet) in at least ~~once~~one melt season between 2016 and 2024, whereas only 1,~~671~~670-1,690 km^2 (~0.1% of the ice sheet) was persistently slush in ~~each and~~ every one of the nine melt seasons. The basins that had the largest areas of this highly persistent slush (i.e. with slush present in every melt season) were the NE and NO, with 920-930 km^2 and 490-500 km^2, respectively. In the SW basin, despite having one of the highest mean slush areal extents over the nine-year period (11,~~550~~530-11,700 km^2), only ~~51~~50-52 km^2 of this area was persistent slush in every melt season. The SE basin experienced both the lowest mean slush areal extent (1,730-1,750 km^2) and the smallest area in which slush reoccurs in the same location in every melt season (43-44 km^2).

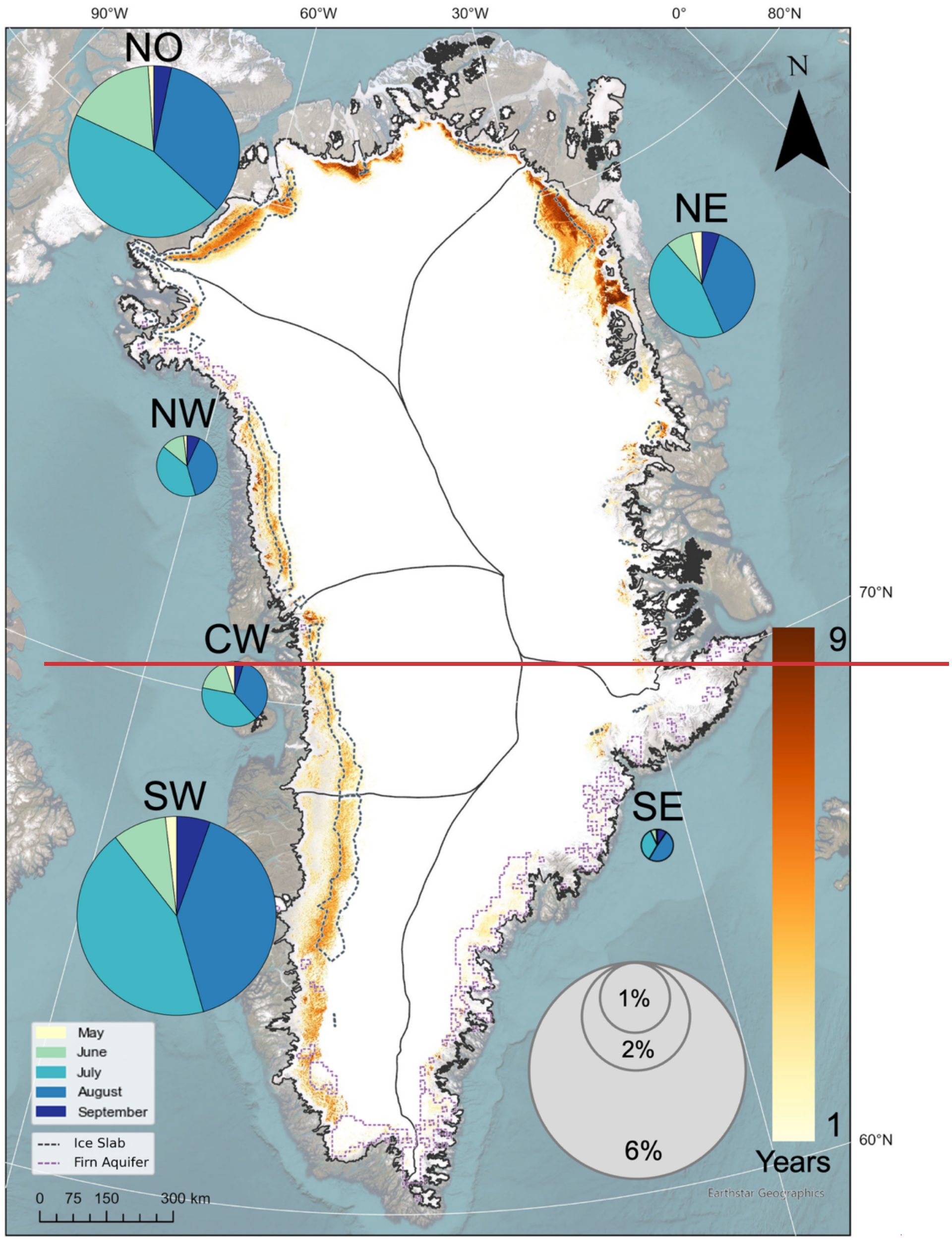

Slush occurrence was concentrated predominantly over bare ice regions, defined here as areas outside the late-summer firn extent where glacier ice is seasonally exposed at the surface, with ~71% (106,630-108,230 km²) of all mapped slush occurring in these regions compared to ~29% (42,730-43,380 km²) over firn-covered areas mapped by Vandecrux et al. (2019). This partitioning strengthened with increasing persistence, with the proportion of mapped slush occurring outside the firn zone increasing from ~62% (47,760-48,480 km²) for 1-2 year persistent slush, to ~78% (39,730-40,330 km²) for 3-5 year slush, and

~91% (19,130-19,420 km^2) for the most persistent (6-9 year) slush, indicating that long-lived slush is increasingly associated with the bare-ice zone. Within the firn zone, overlap with firn aquifers (Miège et al., 2016) remained limited, accounting for only ~6% (8,610-8,740 km^2) of total mapped slush.

Overlap between our mapped slush and the ice slab extents mapped by Jullien et al. (2023) was substantial, ranging from a low-end estimate of ~27% (40,520-41,130 km^2) to a high-end estimate of ~30% (45,030-45,710 km^2) of all slush occurring over mapped slabs, where this range reflects uncertainty in our slush mapping (Section 2.4.1). This slush-slab coincidence increased with time of slush persistence, from a low-end estimate of ~ 19% (15,030-15,260 km^2) to a high-end estimate of ~ 22% (17,540-17,810 km^2) for 1-2 year persistent slush, and from a low-end estimate of ~37 % (7,790-7,910 km^2) to a high-end estimate of 39% (8,060-8,190 km^2) for the 6-9 year persistent slush. Notably, a further ~15% (22,320-22,650 km^2) of all mapped slush occurred within the firn zone but outside both mapped aquifer and slab extents.

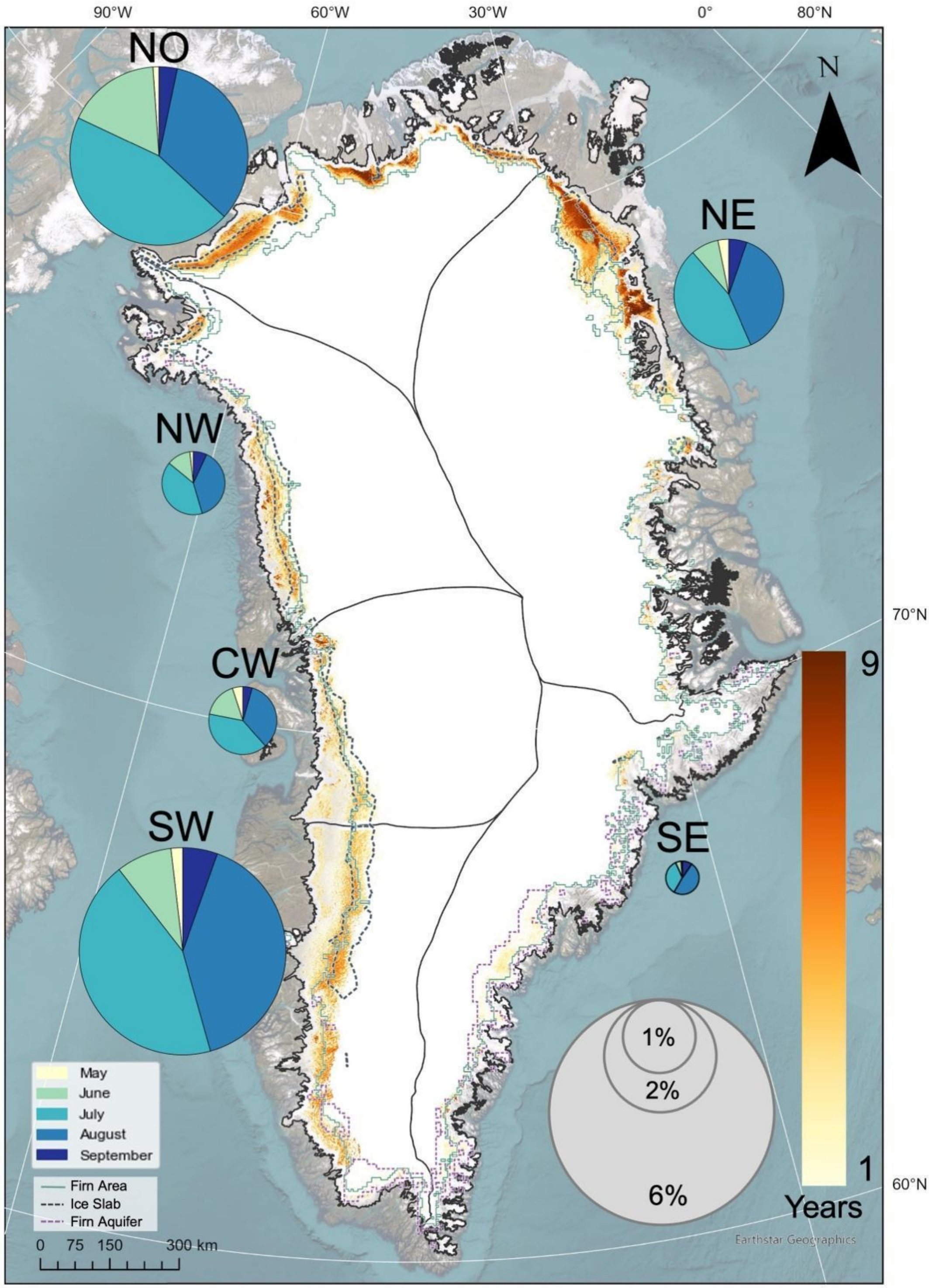
90°W
60°W
30°W
0°
80°N
70°N
60°N
N
NO
NE
NW
CW
SW
SE
9
1
Years
1%
2%
6%
May
June
July
August
September
Firn Area
Ice Slab
Firn Aquifer
0 75 150 300 km
Earthstar Geographics

Figure 3. Slush persistence (years) and mean areal extent (% basin area) across GrIS basins during summers (1 May to 30 September) from 2016-2024. Slush persistence is represented by the colour bar on a scale from 1 year (light yellow) to 9 years (dark orange). The mean slush areal extent for each basin as a percentage of the total basin area, from 2016-2024, is illustrated by the area of the circles. Within each circle, pie charts display the mean monthly distribution of slush areal extent averaged over all melt seasons. The green outline depicts mean firn extent (2000 - 2017) from Vandecrux et al (2019). Dark grey dashed outlines depict ice slab extents from 2010~~–~~-2018 (Jullien et al., 2023), and purple dashed outlines depict firn aquifer extents from 2010~~–~~-2014 (Miège et al., 2016). Base map source: Esri.

3.2. Ice-sheet-wide inter- and intra-annual variability in slush areal extent and elevation

The areal extent of slush across the GrIS varied considerably from year to year~~ across the GrIS~~, closely reflecting interannual variability in surface melt derived from RACMO (Noël et al., 2019) (Fig. 4). ~~Across the ice sheet, maximum seasonal slush extent was strongly correlated with mean May September surface melt (R^2 = 0.91, p < 0.001; Fig. S4a), whereas the relationship with mean air temperature was weaker (R^2 = 0.42), and only significant at p < 0.1 (Fig. S4b).~~

The maximum seasonal areal extent (i.e., the composite slush area from May~~–~~-September) was lowest in 2018, the ~~weakest~~least intense melt season of the study period (Fig. 4c), when slush covered ~~just~~ 20,~~500~~460-20,770 km² (~1.2% of the ice sheet; Fig. 4a~~–~~-b) and RACMO melt anomalies were ~~~15~~2.5 mm w.e. below the ~~1958–2015~~1960-89 mean. The largest extent occurred in 2019, the strongest melt year (Fig. ~~4c~~4b), when slush covered 90,~~300~~120-91,470 km² (~5.2% of the ice sheet) and melt anomalies reached ~~~40~~10 mm w.e. above the 1960-89 mean (Fig. ~~4c~~4b). No statistically significant temporal trend in the maximum seasonal areal extent of slush over the whole ice sheet was observed over the study period.

Superimposed on these interannual variations in slush areal extent from 2016-2024 was a consistent seasonal pattern, with lowest average slush ~~areal~~ extents in May and September (typically a mean of < 0.2% of the ice sheet area over the ~~9~~nine years) and peaks in July (1.7%) and August (1.6%) (Fig. 3). This broad seasonal cycle of low early- and late-season ~~areal~~ extent and mid-summer maxima was a defining feature throughout the study period~~, and consistent with RACMO-derived surface melt and air temperature anomalies, relative to the 1958–2015 climatological mean (Fig. 4b and c).~~. The seasonal cycle was most pronounced in the highest melt year, 2019, when slush reached its greatest extents in July (54,~~200~~090-54,910 km²) and August (67,~~200~~070-68,070 km²) ~~areal extents~~ (Fig. 4b). However, a notable departure from this cycle occurred in September 2022, when slush ~~areal~~ extent (15,970-16,~~000~~210 km²) surpassed that of August by ~4,700 km² (Fig. 4b~~), consistent with a +3°C September air temperature anomaly relative to 1958–2015 mean (Fig. 4d~~).

~~Seasonal~~Interannual variability was also evident in the maximum elevation reached by slush each melt season~~. It fluctuated markedly between years~~ (Fig. 5a), ranging from below 1,300 m a.s.l. in the lowest melt year (2018) to above 1,800 m a.s.l. in the highest melt year (2019). We do not find a statistically significant temporal trend in ~~the~~ maximum slush elevation ~~from~~

~~2016 – 2024~~ at the ice-sheet scale~~, although we do find a significant positive relationship between maximum slush elevation and maximum slush areal extent across the ice sheet (p < 0.05).~~ from 2016-2024.

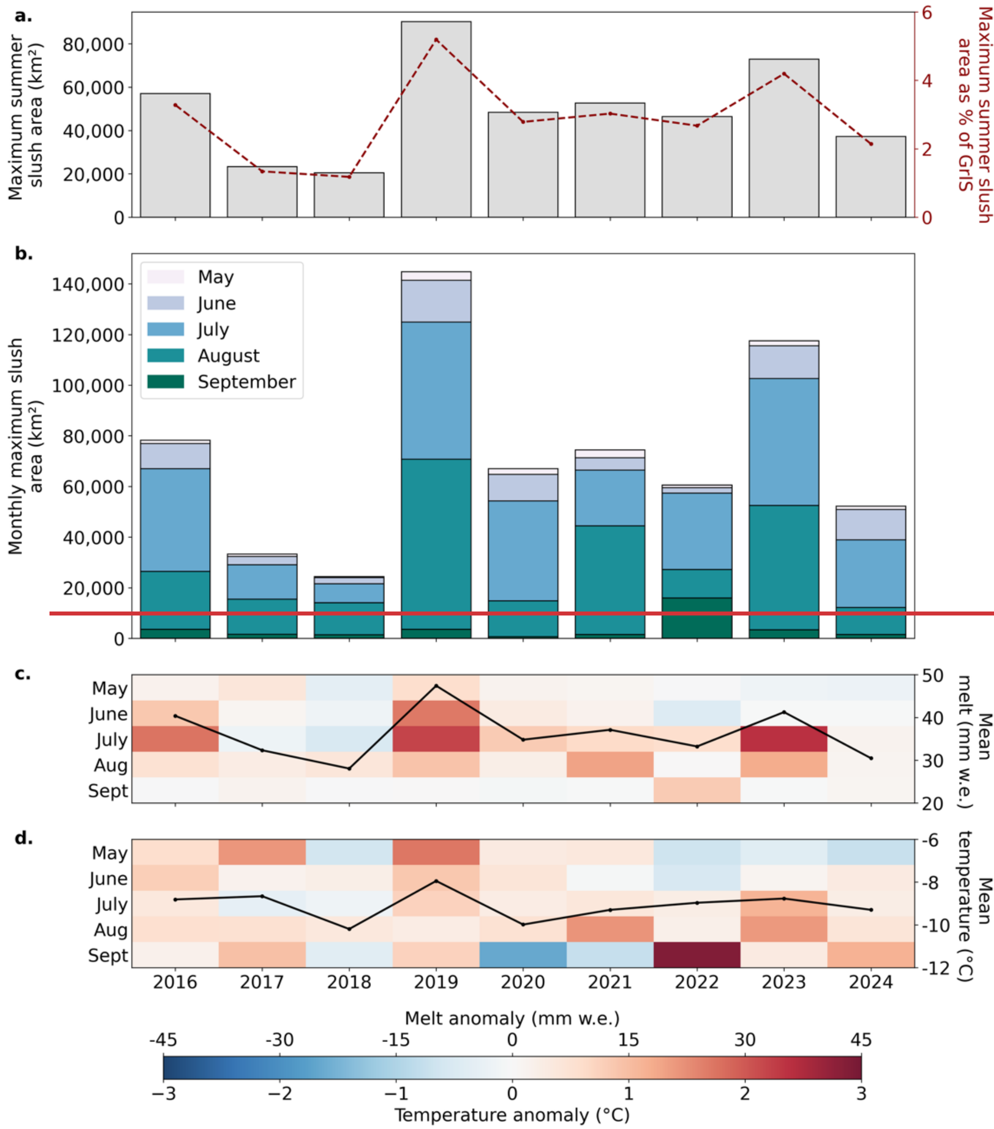

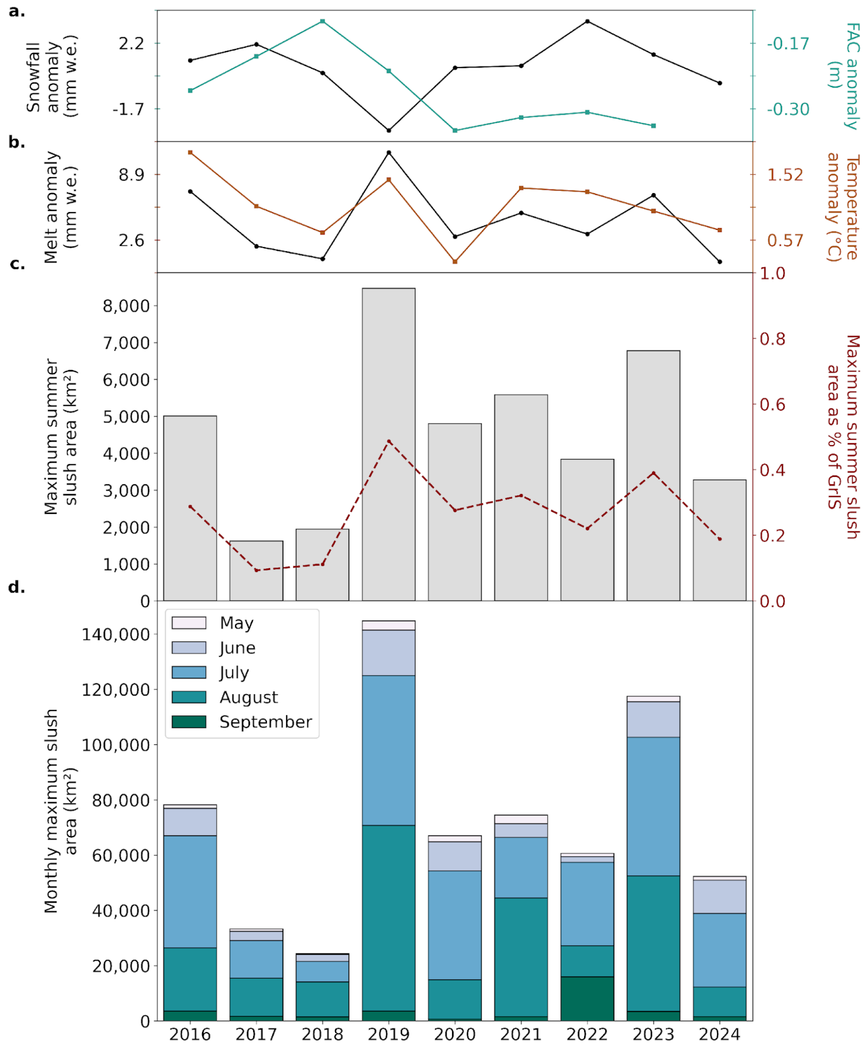

Figure 4. ~~Maximum~~ Mean annual climate and slush ~~area~~variability across the GrIS from 2016~~–~~–2024. a) Snowfall anomalies (black) and FAC anomalies (teal) relative to the 1960-1989 mean. b) Melt anomalies (black) and near-surface air-temperature anomalies (orange) relative to the 1960-1989 mean. c) Maximum summer slush ~~areal extent from~~ area (May~~–~~–September ~~(~~) shown as absolute area (left y-axis, grey bars) and as a percentage of total ice sheet area (right y-axis; dashed dark red line). ~~b)~~d) Stacked monthly maximum slush area~~, stacked (~~ for May~~–~~–September~~) for~~ in each year ~~c) Melt anomalies relative to the 1958–2015 monthly mean for each summer month and year from 2016-2024, with mean seasonal~~. Snowfall, melt ~~indicated by the black line (right y-axis). d) Near-surface air-temperature anomalies relative to the 1958–2015 monthly mean for each summer month and year from 2016-2024, with mean summer~~, and near-surface air temperature ~~indicated by the black line (right y-axis). Melt and air temperature data~~ are derived from RACMO~~.~~, while FAC is derived from the IMAU FDM (available through 2023 only).

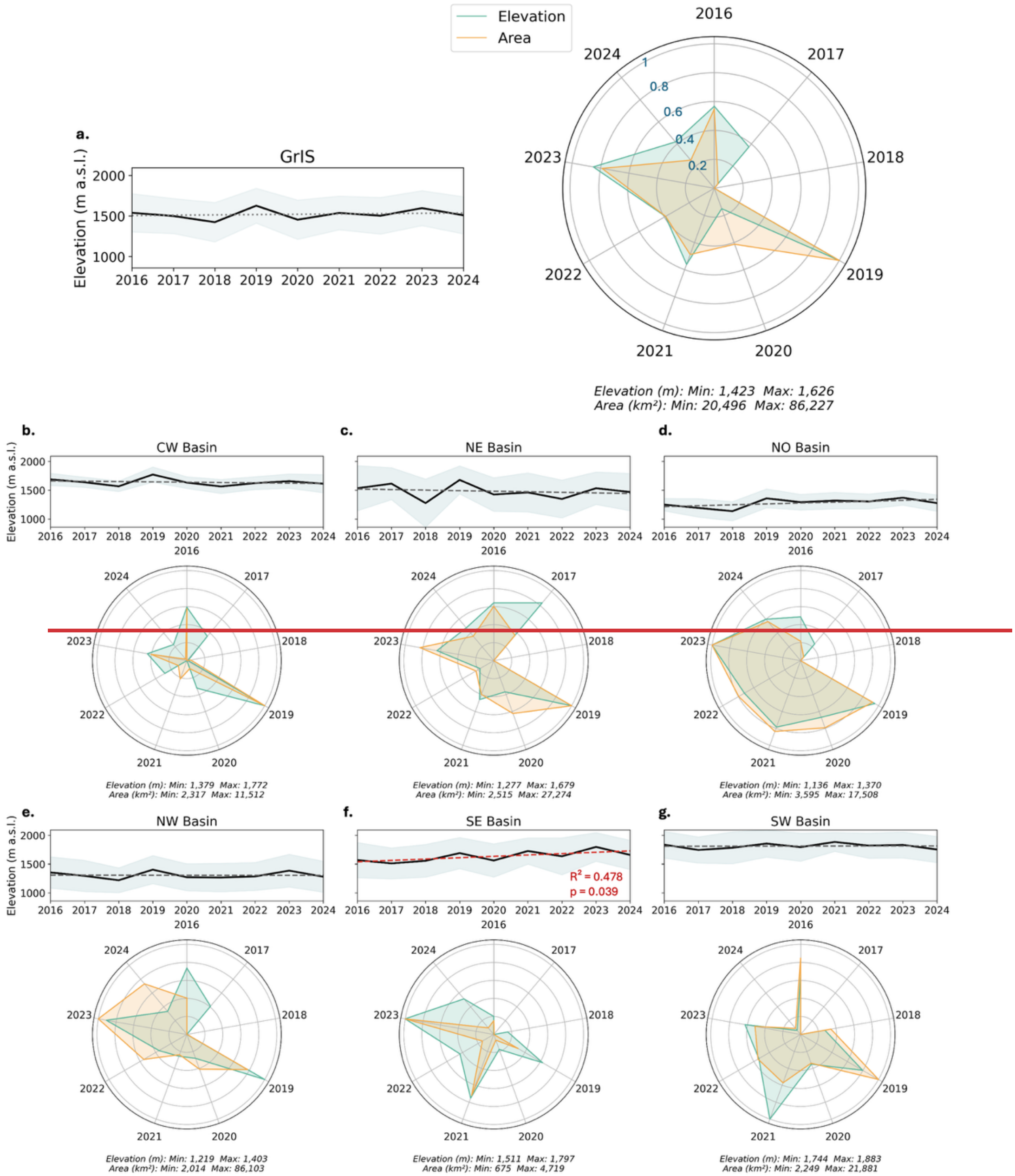
Elevation
Area
a.
GrIS
Elevation (m a.s.l.)
Elevation (m): Min: 1,423 Max: 1,626
Area (km²): Min: 20,496 Max: 86,227
b.
CW Basin
Elevation (m): Min: 1,379 Max: 1,772
Area (km²): Min: 2,317 Max: 11,512
c.
NE Basin
Elevation (m): Min: 1,277 Max: 1,679
Area (km²): Min: 2,515 Max: 27,274
d.
NO Basin
Elevation (m): Min: 1,136 Max: 1,370
Area (km²): Min: 3,595 Max: 17,508
e.
NW Basin
Elevation (m): Min: 1,219 Max: 1,403
Area (km²): Min: 2,014 Max: 86,103
f.
SE Basin
R² = 0.478
p = 0.039
Elevation (m): Min: 1,511 Max: 1,797
Area (km²): Min: 675 Max: 4,719
g.
SW Basin
Elevation (m): Min: 1,744 Max: 1,883
Area (km²): Min: 2,249 Max: 21,881

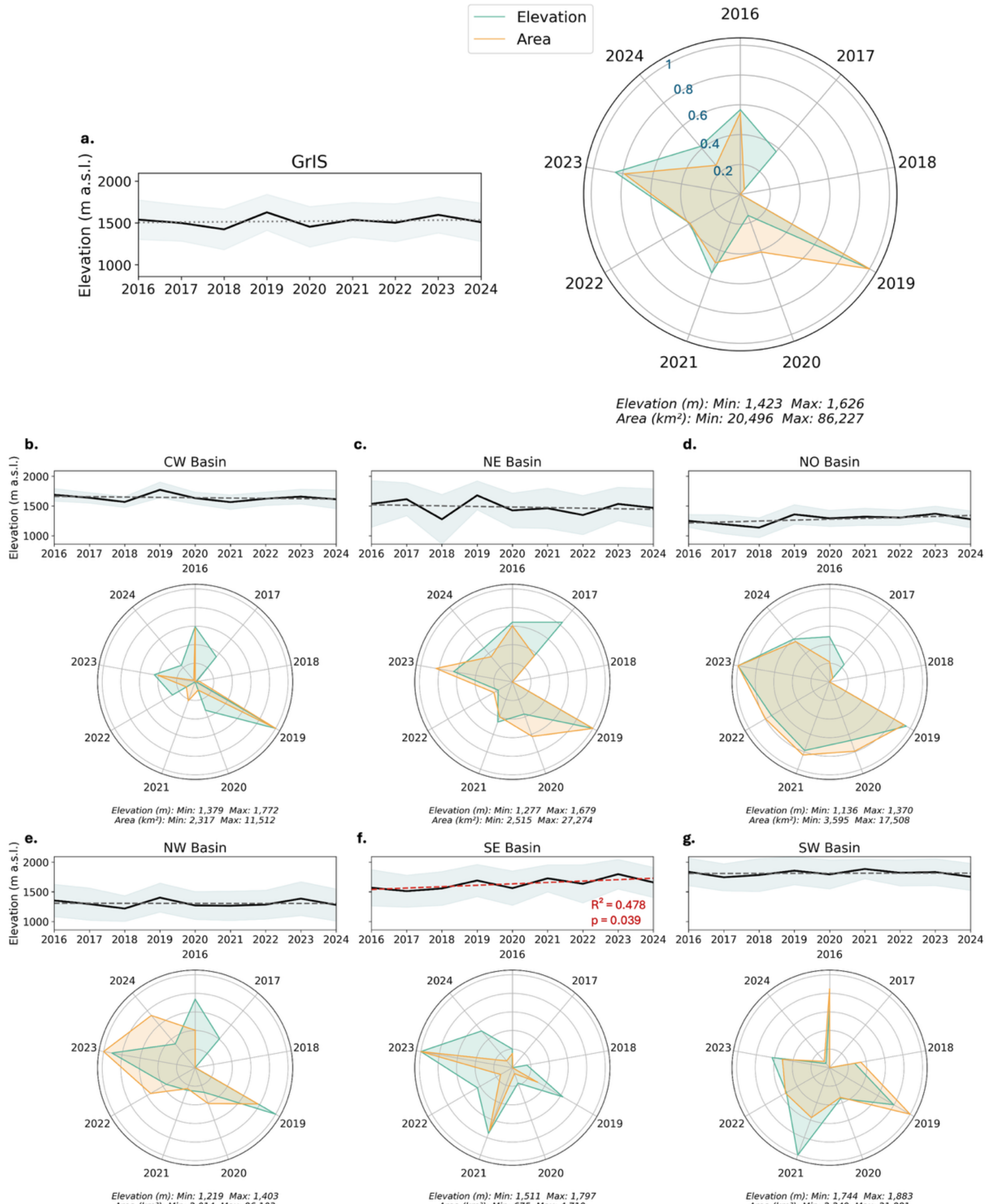

Figure 5. Interannual variability in slush elevation and area from 2016-2024. Panel ~~(~~a) shows ice-sheet-wide results, while panels ~~(~~b~~–~~)-g) depict regional results for the six basins~~ (CW, NE, NO, NW, SE, SW)~~.. Within each subplot, the line graph shows mean maximum slush elevation (m a.s.l.) from 2016-2024 with ± 1 standard deviation shading and a fitted linear trend line (dotted: red if statistically significant at $p < 0.05$, grey if not). The radar chart in each subplot shows the mean annual maximum slush elevation and area from 2016~~–~~-2024, with both variables normalised through scaling from 0 to 1, representing the minimum and maximum observed values, respectively.

3.3. Regional inter- and intra-annual variability in slush areal extent and elevation

At the regional scale, interannual variability in slush areal extent broadly echoed the ice-sheet-wide pattern over the nine-year period (Section 3.2), though the magnitude and precise timing of changes differed by region (Fig. 6). In the highest melt year of 2019, all drainage basins experienced peak or near-peak slush ~~areal~~ extent: the SW reached a maximum seasonal ~~areal~~ extent of 22,~~530~~490-22,820 km^2 ~~(i.e.,~~ (~10.7% of ~~the~~ basin area), the NE 27,~~280~~230-27,630 km^2 ~~(~~(~5.6%), the NO 16,~~460~~430-16,670 km^2 ~~(~~(~6.8%), the CW 11,~~520~~500-11,670 km^2 ~~(~~(~4.9~~%)~~%), and the NW 10,~~490~~470-10,630 km^2 ~~(~~(~3.8%). Other high-melt years also saw elevated slush ~~areal~~ extent in specific regions. For instance, in 2023, the second greatest melt season in the time series, both the NO and SE basins recorded their maximum slush ~~areas~~extents of the time series ~~(~~, reaching 17,~~520~~490-17,750 km~~^{2}, i.e.,~~^{2} (~7.2% of ~~the~~ basin area) in the NO and 4,~~890~~880-4,950 km^2 ~~and~~ (~1.7%) in the SE~~).~~. Post-2019, the NO basin notably ~~maintains~~maintained a consistently higher slush ~~area~~extent than pre-2019 levels~~,~~; a pattern not observed in any other region.

Regional intra-annual variations in slush areal extent over the nine-year period also demonstrated variations in the timing and magnitude of peak slush area (Fig. 6). August 2019 marked the greatest monthly slush ~~areal~~ extent during the time series for all basins except the SE (Fig. 6): the SW basin contained 17,~~950~~910-18,180 km^2 of slush in August 2019 ~~(~~(~8.5% of ~~its~~basin area), the NE reached ~~~~~20,~~460~~420-20,730 km^2 ~~(~~(~4.2%), the NO ~~~~~12,~~450~~430-12,610 km^2 ~~(~~(~5.1%), the NW ~~~~~8,~~130~~110-8,240 km^2 ~~(~~(~2.9%), and the CW ~~~~~7,~~140~~130-7,230 km^2 ~~(~~(~3.1%). September 2022 saw an atypical late-season resurgence in slush ~~areal~~ extent that was above the time series average across most basins (Fig. 6). Notably, September 2022 was the month of peak slush area for the SW basin (Fig. 6f~~);~~), representing the only instance in the record where the annual maximum occurred in September rather than July or August. The preceding month, August 2022, recorded substantially lower values across all basins (e.g. SW: ~~~~~1,780-1,800 km^2, ~0.8%; NE: ~~~~~2,~~830~~820-2,870 km^2, ~0.6%), highlighting the atypical nature of this late-season peak.

~~Across the six drainage basins, slush areal extent exhibited positive correlations with RACMO-derived mean May–September melt (mm w.e.), with R^2 values ranging from 0.46 (SE) to 0.95 (CW), which were all significant at $p \leq 0.05$ (Fig. S5). In contrast, the relationship between slush extent and mean May–September 2 m air temperature (°C) was not significant in any basin (Fig. S6). These results likely reflect how air temperature is not the sole driver of meltwater (and hence slush) production, and that other components of the surface energy balance play a dominant role.~~

The maximum elevation reached by slush varied markedly between basins and years (Fig. 5). ~~Such elevations were~~Slush generally extended to higher ~~in the highest~~ elevations during high-melt years ~~of~~, including 2019 (e.g., CW: 1,770 m a.s.l~~.,~~.; NE: 1,700 m a.s.l~~.,~~.; NO: 1,370 m a.s.l~~)~~.) and 2023 (e.g~~.~~., SE: 1,800 m a.s.l~~.,~~.; NW: 1,470 m a.s.l~~), and~~.), while maximum elevations were lower ~~in the lower~~ during reduced-melt years ~~of~~such as 2018 and 2020 (e.g~~.~~., NE: 1,290 m a.s.l. in 2018; CW: 1,380 m a.s.l. in 2020). Some basins showed distinct inter-annual changes in maximum slush elevation; for example, in the NE basin, an increase of > 400 m occurred between 2018 and 2019. Notably, peak slush elevation did not always coincide with years of peak slush areal extent; for instance, the SW reached its highest elevation in 2021 (~~1880 m~~1,880 m a.s.l), two years after its areal maximum in 2019 (Fig. 5g). A weak statistically significant increasing temporal trend in maximum slush elevation was observed in the SE basin from 2016 to 2024, with a mean increase of 23.5 m/year ($p < 0.05$, $R^2 = 0.48$; Fig. 5f). No other basins exhibited statistically significant temporal trends between these two variables during the study period.

We found a significant positive relationship between maximum slush elevation and maximum slush areal extent across all basins ($p < 0.05$; Fig. 7). The strength of this relationship varied regionally, with the strongest correlations in the NO ($R^2 = 0.91$) and SE ($R^2 = 0.81$) basins, moderate correlations in SW ($R^2 = 0.70$) and CW ($R^2 = 0.74$), and weaker correlations in NE ($R^2 = 0.60$) and NW ($R^2 = 0.49$). ~~We also found that northern basins (NO, NE, NW) generally sustained higher slush elevations for a given areal extent compared to southern basins (SW, SE, CW).~~

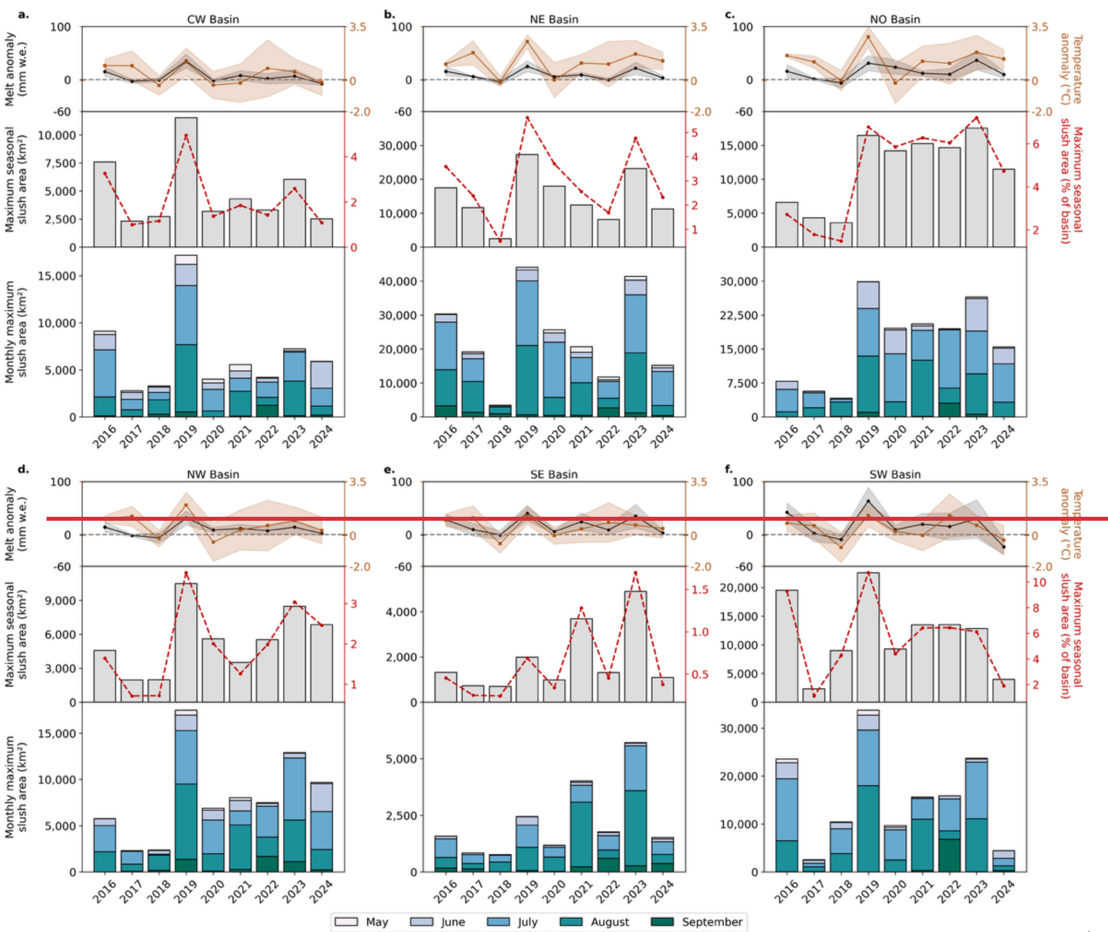

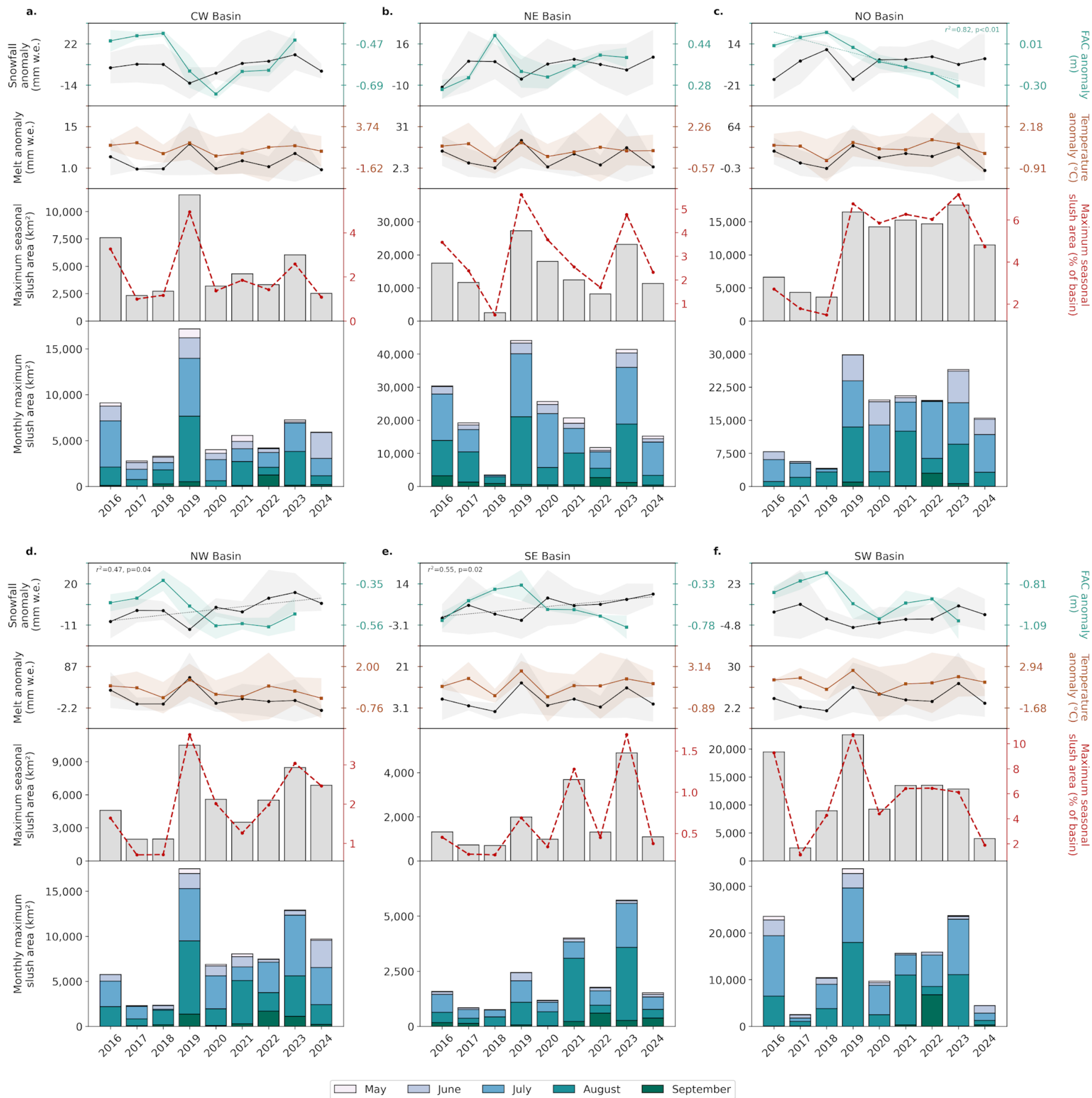

Figure 6. Plots illustrating the total slush area alongside snowfall, FAC, melt~~,~~ and air temperature anomalies from 2016-2024 (FAC available through 2023 only) for the six basins of the GrIS (subplots a - f). Within each subplot, the ~~upper panel displays~~two uppermost panels display RACMO-derived ~~melt (black) and air temperature~~ anomalies ~~(red),~~

~~both~~ averaged over the May~~–~~-September period~~.~~ and expressed relative to the 1960-1989 baseline mean: snowfall (black) and FAC (teal) in the first panel, and melt (black) and air temperature (orange) in the second. Dashed lines indicate statistically significant linear trends ($p < 0.05$) and shaded regions indicate ± 1 standard error of the monthly means. The ~~middle~~third panel shows maximum seasonal slush areal extent from May~~–~~-September as grey bars, with the right y-axis showing this as a percentage of the basin area~~.~~ (dashed red line). The bottom panel shows the total slush area (km^2), segmented by month (May, June, July, August, and September) for each melt season.

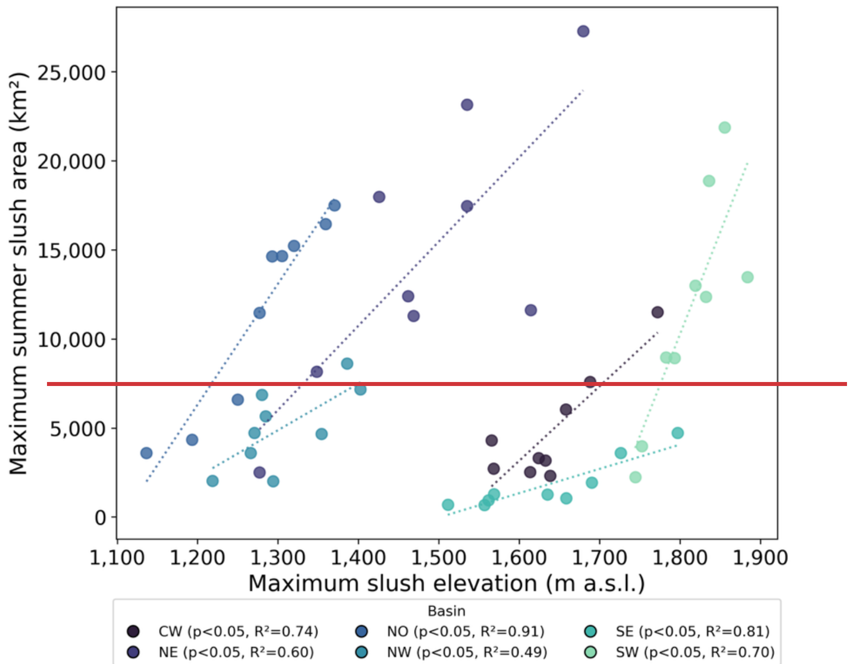

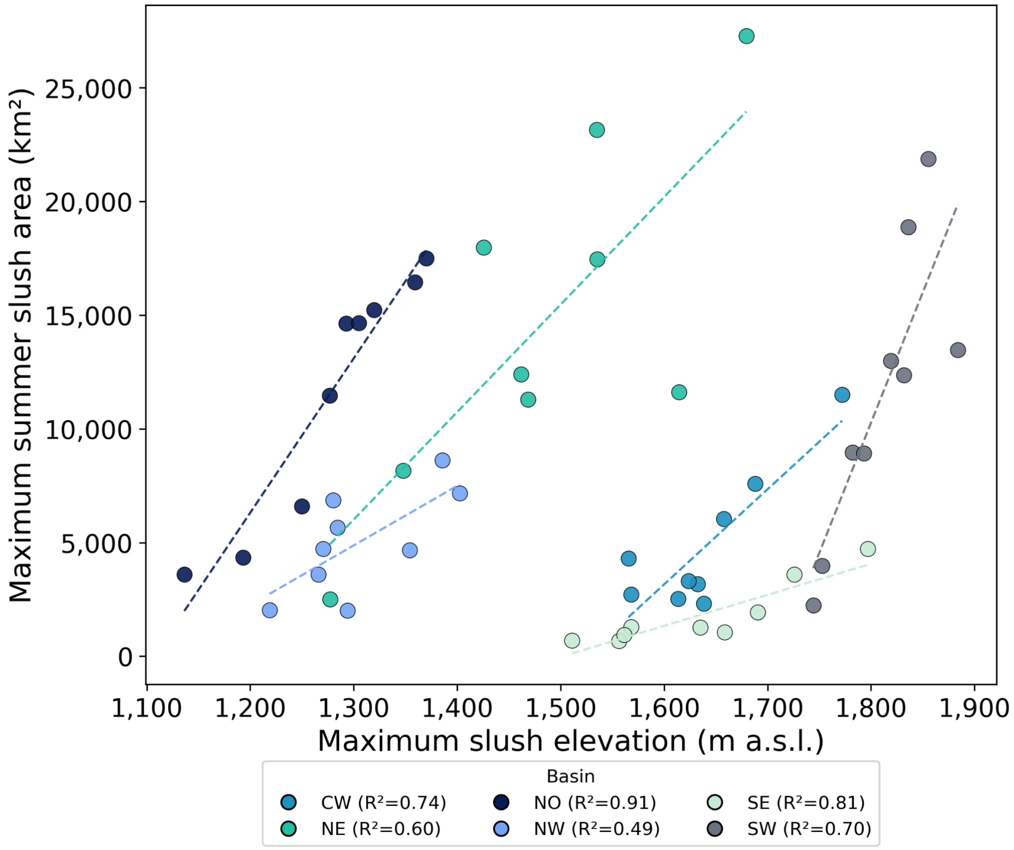

Figure 7. Relationship between maximum slush elevation and maximum areal extent of slush by basin (2016–2024). Coloured points show annual values, with dotted lines indicating least-squares regressions. All relationships are statistically significant (*p* < 0.05).

3.4. Potential controls on interannual and intra-annual variability in slush extent

We investigated potential controls on slush extent at both interannual and intra-annual timescales by using Spearman rank correlations between slush extent and FAC from the IMAU-FDM, together with snowfall, snowmelt, and 2 m air temperature from RACMO. For the interannual analysis, correlations were evaluated at the GrIS-wide scale, with mean May-to-September slush area used as the response variable. Predictor variables for FAC, snowfall, snowmelt, and 2 m air temperature were computed as seasonal means over January-to-March, April-to-June, and May-to-September windows to assess antecedent and contemporaneous relationships with slush extent (Fig. S6). For the intra-annual analysis, correlations were evaluated separately for each GrIS basin. The response variable was monthly slush area; lagged predictor variables were constructed by shifting each basin time series by one month, such that the previous-month value for any given May-to-September observation reflects conditions in the preceding calendar month (Fig. S7-S10).

At the interannual GrIS-wide scale, mean seasonal slush area throughout May-to-September was negatively correlated with FAC across all seasonal windows (Fig. S6), including January-to-March ($\rho = -0.56$, $p < 0.001$), April-to-June ($\rho = -0.57$, $p < 0.001$), and May-to-September ($\rho = -0.59$, $p < 0.001$). Snowmelt was also positively associated with interannual variability in slush extent, with positive correlations identified during January-to-March ($\rho = 0.37$, $p < 0.01$), April-to-June ($\rho = 0.38$, $p < 0.01$), and May-to-September ($\rho = 0.42$, $p < 0.005$). Similarly, slush extent was positively correlated with 2 m air temperature across all seasonal windows, including January-to-March ($\rho = 0.35$, $p < 0.01$), April-to-June ($\rho = 0.46$, $p < 0.001$), and May-to-September ($\rho = 0.43$, $p < 0.01$). Relationships with snowfall were more variable between seasonal windows, with positive correlations identified during January-to-March ($\rho = 0.31$, $p < 0.05$) and April-to-June ($\rho = 0.47$, $p < 0.001$), although no significant relationship was observed for May-to-September snowfall.

At the intra-annual basin-wise scale, monthly slush extent during May-to-September was positively correlated with snowmelt across all basins (Fig. S7), with particularly strong relationships in CW ($\rho = 0.87$, $p < 0.001$), NO ($\rho = 0.78$, $p < 0.001$), and SW ($\rho = 0.76$, $p < 0.001$). Positive relationships were also identified for previous-month snowmelt across all basins, ranging from $\rho = 0.43$ in NO ($p < 0.01$) to $\rho = 0.80$ in SE ($p < 0.001$). 2 m air temperature was positively associated with monthly slush extent across all basins (Fig. S8), with significant correlations ranging from $\rho = 0.63$ in NE ($p < 0.001$) to $\rho = 0.81$ in SW ($p < 0.001$). Similar, but generally weaker, associations were identified for previous-month 2 m air temperature. Negative relationships between monthly slush extent and FAC (Fig. S9) were identified in NE ($\rho = -0.55$, $p < 0.001$), NO ($\rho = -0.49$, $p < 0.005$), NW ($\rho = -0.50$, $p < 0.005$), and SE ($\rho = -0.59$, $p < 0.001$), whereas no significant relationships were identified in CW or SW. Negative relationships with previous-month FAC were weaker, with a significant relationship identified only in SE ($\rho = -0.34$, $p < 0.05$). Relationships with snowfall (Fig. S10) were the most spatially variable, with statistically significant negative relationships observed in NE ($\rho = -0.31$, $p < 0.05$), whereas positive relationships were identified in SE for concurrent ($\rho = 0.31$, $p < 0.05$) and previous-month snowfall ($\rho = 0.48$, $p < 0.001$), and in SW for concurrent snowfall ($\rho = 0.40$, $p < 0.01$).

4. Discussion

To the best of our knowledge, our work forms the first large-scale assessment of slush on the GrIS. ~~Existing~~Prior assessments have almost exclusively focused on well-defined supraglacial meltwater features, specifically, lakes, ~~streams~~channels, and water-filled crevasses (e.g., Zhang et al. 2023, Fan et al., 2025; Melling et al., 2024; Dunmire et al., 2021; 2025) that are somewhat easier to map using traditional thresholding methods. By leveraging ML within a cloud-based framework, we show that slush can be systematically mapped across the entire ~~ice sheet at high spatial resolution.~~GrIS. The resulting nine-year, ice-sheet-wide dataset offers new insight into the spatial variability and persistence of slush, revealing that slush is a widespread and climatically sensitive component of the surface hydrological system ~~feature~~ on the GrIS.

4.1. Slush dominates the areal extent of surface meltwater on the GrIS

Between 2016 and 2024, we show that slush covered a mean area of 2.9% ~~(~~(∼50,400 km^2) of the GrIS each summer, with a peak areal extent of 5.2~~ % (~~% (∼90,300 km^2) in 2019, the year of highest melt in our study period (Figs. 3 and 4). In the same year, Zhang et al. (2023) mapped a maximum area of 9,990 km^2 for lakes, ~~streams~~channels, and water-filled crevasses; slush therefore covered over nine times more of the GrIS than these other meltwater features in 2019. Even in the lowest melt year of our study period, 2018, our mapped slush areal extent (1.2%; ∼20,500 km^2) was over four times greater than the 4,900 km^2 of other meltwater features reported by Zhang et al (2023) for 2018. Studies focusing solely on supraglacial lakes highlight an even greater disparity. Fan et al. (2025) showed that between 1985 and 2023, supraglacial lake area rarely exceeded 3,500 km^2, with a total of ∼3,000 km^2 in 2019. ~~Similarly,~~ Additionally, compared with the ice-sheet-wide supraglacial lake extents reported by Dunmire et al. (2021) ~~reported total supraglacial lake areas~~ of 1,~~242~~240 km^2 in 2018 and 2,~~569~~570 km^2 in 2019~~. In both cases,~~, the total ~~areas of~~ slush ~~observed~~extent mapped in our study ~~exceeded total lake areal extents by ∼~~was approximately 16~~ times~~-fold greater in 2018 and ~~∼~~35~~ times~~-fold greater in 2019.

At the basin scale, our slush areal extent observations also greatly surpass the areal extent of other meltwater features observed previously. For example, for the NE in 2019, we detected a maximum slush areal extent of 27,280 km^2, whereas Zhang et al. (2023) reported just 820 km^2 of other meltwater features in this basin; a more than 30-fold difference. Although the aforementioned cross-study comparisons for the GrIS reflect differing methodologies, they are used here to provide first-order context for the relative spatial extent of slush compared to other surface meltwater features. Given that slush has been largely overlooked in previous studies, this comparison highlights its widespread presence across the GrIS.

~~Although the aforementioned cross-study comparisons reflect differing methodologies; we use them to illustrate relative scale. These comparisons demonstrate that slush is the most extensive surface meltwater feature on the GrIS, especially since our slush areas likely represent lower bounds, as optical sensors capture only surface slush and cannot detect subsurface saturation. The true difference in areal extents between slush and other meltwater features may therefore be even larger than estimated here.~~

The dominance of slush on the GrIS relative to lakes also contrasts strongly with Antarctic ice shelves where slush and lakes occupy approximately equal areas, with slush contributing ∼50% of peak-summer (January) meltwater extent across 57 ice shelves (Dell et al., 2024). The higher slush proportion on the GrIS likely reflects fundamental differences in glaciological setting and climate relative to Antarctic ice shelves, with the former experiencing particularly stronger melt intensity (van den Broeke et al., 2023; Hanna et al., 2024), reduced FAC (Firn Symposium Team, 2024), widespread bare-ice exposure (Ryan et al., 2019), and recurrent near-surface saturation due to ice slabs and lenses (Culberg et al., 2021; Machguth et al., 2016). Together, these factors allow slush to expand across broad contiguous zones on the GrIS. Contrastingly, in Antarctica, lake and slush formation is predominantly restricted to flatter ice shelves (Stokes et al., 2019), where lower melt magnitudes, colder mean conditions, and almost complete refreezing of meltwater within the firn (van den Broeke et al., 2023) limits the spatial extent and persistence of all forms of surface meltwater, compared to the GrIS. As Antarctic surface hydrology may increasingly come to resemble present-day Greenland under future warming (Bell et al., 2018; Mottram et al., 2025), improving process-level understanding of slush dynamics across both ice sheets is an urgent research priority.

4.2. Slush is most extensive in the western and northern basins

Our observations reveal that slush is most extensive in the western (notably the SW) and northern basins of the GrIS, and least extensive in the eastern and southeastern basins. This distribution aligns with observations from previous supraglacial hydrology studies, which report more extensive meltwater features in west Greenland, particularly supraglacial lakes (e.g., Selmes et al., 2011; Hu et al., 2022; Zhang et al., 2023; Fan et al., 2025; Dunmire et al., 2021; 2025).

In the SW basin, low-angle slopes, broad ablation zones (Ryan et al., 2019), and high melt rates (Mikkelsen et al., 2016; van As, 2017) create conditions that likely allow slush to extend further inland than in other regions. A disproportionate loss of ~~firn air content~~FAC relative to other regions (Vandecrux et al., 2019) may also promote widespread surface saturation and slush formation in the SW~~.~~ by reducing the capacity of the firn column to accommodate meltwater. Although these conditions favour extensive inland slush in much of the SW basin, the western margin coincides with the ~~“~~‘dark ~~zone”~~zone’ (Tedstone et al., 2017), where limited snow cover, high melt rates, and prolonged bare ice exposure (Feng et al., 2024) may restrict slush formation, ~~producing a~~ consistent with the distinct stripe of low slush persistence ~~parallel with~~that we identify along the western ice-sheet margin (Fig. 3).

The dominance of slush ~~we observed~~ in the western and northern regions ~~of the ice sheet~~ may also ~~be linked to the prevalence of pre-existing low-permeability ice slabs. Ice slabs inhibit~~reflect the distribution of surface and sub-surface structures that restrict vertical meltwater ~~percolation and~~ infiltration. A substantial proportion of mapped slush (~71%) occurs outside the firn zone, within the bare-ice region, where the ice surface itself forms an inherently impermeable boundary to downward percolation. An important control on slush distribution also appears to be the presence of sub-surface ice slabs, which act as shallow permeability barriers within the firn column. By restricting vertical percolation, slabs promote sustained saturation of the ~~firn above, leading to slush formation that encourages~~overlying firn and favour lateral meltwater ~~transport and runoff~~ routing, creating conditions conducive to recurrent slush formation (Machguth et al., 2016; MacFerrin et al., 2019; Jullien et al., 2023). ~~We calculate that about~~Approximately 30% ~~(45,100 km^2)~~ of Greenland's mapped slush area ~~lies above ice slabs,~~ overlaps with slab extents, with most of this concentrated in the western and northern basins (Fig. ~~3). An additional ~10% (8,330 km^2) of slush forms above firn aquifers (i.e., saturated subsurface reservoirs), which are mainly present in the SE basin and may contribute to slush formation via their rising water table during intense melt events~~3). Areas of longer persistence of slush in these regions are often coincident with slab presence, potentially reflecting a positive feedback in which meltwater supplied by lateral flow through the slush zone ponds in shallow-slope zones above the slab, where repeated refreezing locally thickens the slab and reinforces the shallow permeability barriers that favour recurrent slush formation, as observed by Tedstone et al. (2025).

Unlike slabs, firn aquifers are characterised by the deep infiltration of meltwater into temperate firn and long-term sub-surface water storage rather than shallow blockage of vertical flow (Forster et al., 2014; Miege et al., 2016~~). The remaining 60% of slush areal extent occurs in regions lacking underlying low-permeability layers (Fig. 3), instead forming when when the rate of meltwater production exceeds the firn's capacity to absorb and facilitate water percolation. Achieving full firn saturation is more challenging under these conditions, as the firn must become saturated at depth, which typically occurs when preferential flow fingers are overwhelmed)~~, and ~~a uniform wetting front saturates the surface layers (~~can host ice layers (e.g., Miller et al., 2020). Comparatively limited overlap of aquifers with mapped slush suggests that they do not appear to exert the same sustained control on slush persistence as shallow impermeable ice layers.~~Clerx et al., 2022; 2024).~~

~~Persistence patterns mirror these distributions (Fig. 3): slush is generally more persistent above ice slabs, reflecting the sustained saturation they promote, whereas slush above firn aquifers appears less persistent, consistent with their more variable hydrological influence.~~

~~Together, the spatial and temporal persistence patterns that we observe indicate that while pre-existing low-permeability structures may exert a control on where slush is most stable and recurrent, extensive slush formation does also occur in regions without slabs or aquifers when melt intensity overwhelms firn storage capacity. However, fully resolving the physical coupling between slush occurrence, firn stratigraphy, permeability, and refreezing capacity requires dedicated future work. The dataset presented here provides a new observational foundation for such integrative analyses.~~

Notably, a non-trivial fraction of all mapped slush (~15%) occurs within firn areas outside both mapped ice slab and firn aquifer extents, much of it concentrated in western Greenland where slush persistence is highest. While recurrent slush formation in bare ice regions is expected due to the impermeable ice surface, these observations indicate that persistent slush can also develop in firn regions lacking extensive perennial low-permeability units. In these settings, smaller-scale ice lenses and contrasts in firn density and grain size may locally restrict vertical percolation, promoting lateral spreading and near-surface saturation, consistent with experimental observations from Greenland firn (Humphrey et al., 2021). Periods of intense melt may further enhance these effects where meltwater production exceeds local infiltration capacity. Together, these patterns suggest that finer-scale firn stratigraphic heterogeneity may exert an important control on recurrent slush formation across parts of the ice sheet.

4.3. Slush reaches higher elevations and is greater in areal extent during extreme melt years

In extreme melt years (notably 2019 and 2023; the highest and second highest melt seasons in our time series, respectively), slush both reaches higher elevations and is more areally extensive than in cooler, low-melt years (e.g., 2018; Figs. 5 and 6), which also mirrors the established tendency for supraglacial lakes to appear at higher elevations in warmer years (Sundal et al., 2009; Liang et al., 2012; Lüthje et al., 2006; Leeson et al., 2015; Glen et al., 2025). Under typical conditions, we show that variability in the areal extent in slush follows a predictable seasonal cycle, forming in May, peaking in areal extent and maximum elevation in July, and decreasing in area during the autumn freeze-up, similar again to the behaviour of supraglacial lakes (e.g., Otto et al., 2022; Yang et al., 2021; Glen et al., 2025). During extreme high melt years such as 2019, this seasonal cycle is amplified, with sustained high air temperatures combined with melt-albedo feedbacks producing prolonged, intense melt (Sasgen et al., 2020; Tedesco ~~&~~and Fettweis, 2020; Hanna et al., 2021), which likely drove 2019 to have the most extensive and furthest inland slush areal extents in our record. In contrast, we suggest that the atypical pattern in 2022 resulted from a late-season, ~~anonymously~~anomalously warm and rainy event in September 2022 that triggered ice-sheet~~–~~-wide melt and delayed late-season freeze-up (Moon et al., 2022; C3S, 2023), enabling the sustained slush presence that we observed into ~~October~~late-September 2022.

Despite the strong interannual variability in slush elevation and area that we observe, our nine-year record reveals no statistically significant temporal trend in slush area or elevation at either ice~~-~~ sheet or regional scales, except from a weak elevation increase in the SE basin (R^2 = 0.~~478~~48, $p < 0.05$). These results are consistent with Machguth et al. (2022), who, over a similar length study period (2012~~–~~-2021), found no significant change in maximum slush elevation on the western GrIS, but observed pronounced intra-seasonal variability. Multi-decadal studies, however, have reported increases in meltwater feature area and elevation over time. For example, Fan et al. (2025) documented an ice-sheet-wide supraglacial lake area increase of ~50.5 $km^2 yr^{-1}$ from 1985~~–~~-2023, while Tedstone and Machguth (2022) reported increases in visible runoff limits of ~242 m (west), 194 m (north), and 59 m (northeast) between 1985~~–~~-2020. These findings suggest that while inter- and intra-annual variability dominate decadal slush records, slush is nonetheless likely to follow the broader trajectory of increasing area and elevation over multi-decadal timescales.

Our observations suggest that extreme melt events not only drive widespread slush formation through direct surface melt, but they may also ~~precondition~~alter firn structure in ways that may amplify future slush formation, effectively preconditioning the ice sheet for slush recurrence in subsequent melt seasons~~ driving greater persistence.~~. For example, the ~~NO~~northern basin exhibited elevated slush areal extent in all years after the extreme 2019 melt season (Fig. 6c), even when melting was low. This is suggestive of a ‘legacy’ effect, where slush that formed during 2019 refroze to produce low-permeability firn and/or thicken pre-existing ice slabs, reducing firn infiltration capacity. ~~In later years~~This interpretation is further supported by the strong and statistically significant decline in FAC from 2016 to 2023 (R^2 = 0.82, $p < 0.01$; Fig. 6). Under these reduced-storage conditions, only saturation of the seasonal snowpack ~~needs to saturate~~may be required to regenerate slush~~. This~~ in subsequent years. Our interpretation is consistent with recent work by Rawlins et al. (2023), who documented earlier melt onset and prolonged melt seasons in northern Greenland following major slush events in previous years.

~~The sensitivity of slush formation to extreme melt events, as observed in this study, highlights its potential for rapid areal expansion under continued atmospheric warming. Combined with Arctic amplification and ice–climate feedbacks driving longer and more frequent intense melt seasons on the GrIS (Hanna et al., 2024), this suggests that slush may not only expand rapidly during peak melt events but may also persist later into the season due to delayed freeze-up, thereby extending its role as an active component of the hydrological regime. These changes may alter surface and subglacial meltwater routing, impact ice dynamics and mass balance, and ultimately affect the ice sheet's contribution to sea-level rise.~~

~~4.4.~~**4.4. Slush variability is associated with meltwater supply, firn storage capacity, and atmospheric forcing**

We find that slush variability is strongly associated with meltwater supply, firn storage capacity, and atmospheric forcing across both interannual and intra-annual temporal scales. At the interannual GrIS-wide scale, the negative relationships with FAC we find across January-to-March, April-to-June, and May-to-September suggest that years with reduced firn pore space are associated with more extensive summer slush development, because less meltwater can be retained and refrozen within the firn before near-surface saturation is reached. This is consistent with the established role of firn air content as a first-order control on meltwater retention capacity across Greenland (e.g., Vandecrux et al., 2019), and with wider evidence from Antarctic ice shelves that FAC can act as a threshold control on the development of surface meltwater once storage capacity is sufficiently reduced (Dell et al., 2024). Enhanced snowmelt may then act as the principal driver translating this storage deficit into observable slush extent, as increased meltwater supply is more likely to overwhelm the reduced pore space and promote sustained surface saturation and lateral redistribution of water. Significant positive relationships with 2 m air temperature were identified across all seasonal windows, suggesting that atmospheric warming contributes to interannual slush variability, likely through its direct influence on melt production; however, the comparatively stronger relationships with FAC suggest that variability in slush extent at the interannual GrIS-wide scale is more directly associated with firn storage capacity than with temperature alone. The weaker positive relationships with snowfall suggest that fresh snow may temporarily enhance near-surface water retention and help preserve slush once melting begins.

At the intra-annual basin-wise scale, strong correlations with same-month and previous-month snowmelt across all basins indicate that slush extent tracks melt forcing closely, and that antecedent melt conditions also contribute to monthly slush variability, potentially reflecting persistence of wetted firn into subsequent months even as melt intensity weakens. Air temperature shows similar positive associations across all basins. Negative relationships with same-month FAC across most basins suggest that reduced pore space promotes melt-season slush development, though the absence of significant FAC relationships in CW and SW likely reflects the widespread FAC depletion documented across western Greenland (Vandecrux et al., 2019), where meltwater supply rather than storage capacity becomes the more direct control. Snowfall relationships varied regionally (negative in NE, positive in SE and SW) consistent with snowfall influencing slush development through different mechanisms: fresh snow can enhance near-surface water retention and facilitate slush formation (The Firn Symposium Team, 2024), but may also increase storage capacity or suppress melt in other settings, reducing slush extent.

4.5. Slush has implications for surface energy balance and hydrological modelling

Slush plays a key role in regulating ~~glacier~~ice sheet surface energy balance and meltwater pathways, and accurately representing its presence and dynamics in models of surface energy~~-~~ balance (e.g. ~~Noel~~Noël et al., 2019; Huai et al., 2020), lake formation (e.g. Law et al., 2020) and ~~surface~~ hydrological routing (e.g. Banwell et al., 2012; Leeson et al., 2012~~) models~~; Gantayat et al., 2023) is essential to capture realistic albedo~~–~~-melt feedbacks, meltwater storage capacity, and connectivity between supraglacial hydrological features. ~~Incorporating time-varying slush layers can improve estimates of surface albedo reduction (Ryan et al., 2025) and melt (Dell et al., 2024), while accounting for its temporary storage and connectivity functions may improve predictions of surface and subglacial water routing, ice dynamics, and the ice sheet's seasonal evolution (e.g., de Fleurian et al., 2018). Observations such as those presented here~~Our new ice-sheet-wide observations presented in this study provide a well-constrained input to refine these hydrological models and better capture the complex interactions between meltwater and ice~~-~~ sheet processes.

Our ice-sheet-wide slush observations provide a first opportunity to approximate its potential radiative and hydrological consequences at scale. Using the empirical meltwater-albedo framework of Ryan et al. (2025) as an upper-bound analogue, the slush extents derived here imply a mean ice-sheet-wide excess energy absorption of 134 PJ d^{-1} over 2016-2024 (range 53-249 PJ d^{-1}), peaking in the extreme melt year of 2019 (Section S3). These estimates should be treated as upper bounds due to the optical differences between slush and open water. Nevertheless, the larger areal extent of slush relative to open meltwater suggests that its contribution to surface darkening and melt amplification may be substantial, reinforcing the need to explicitly incorporate slush into future surface energy balance frameworks. Additionally, current regional climate model frameworks, including RACMO and MAR, typically partition meltwater directly between vertical refreezing and runoff without representing a transient phase of lateral meltwater transport within surface slush layers (Noël et al., 2018; Fettweis et al., 2017). Our results suggest that this omission may distort both runoff timing and near-surface retention. For example, in the CW basin during 2019, slush-covered pixels accounted for ~28% of annual modelled runoff and ~13% of modelled refreezing, despite occupying only ~5% of RACMO grid cells (Section S4). This disproportionate influence highlights how slush represents a transient phase of meltwater retention and lateral routing before export or refreezing (e.g., Clerx et al., 2022; Tedstone et al., 2025), a process likely to become increasingly important as ice slabs expand inland (Jullien et al., 2023) and slush migrates to higher elevations (Tedstone and Machguth, 2022) with continued atmospheric warming.

Although the analyses presented here are first-order and should not be interpreted as fully constrained physical estimates, they nevertheless demonstrate that slush may exert an important influence on the surface energy balance, meltwater routing, and runoff generation across the GrIS. Future work explicitly coupling slush processes within physically based surface mass-balance and hydrological models will therefore be important for constraining its role in ice sheet evolution under continued warming.

5. Conclusion

We present the first ~~high spatial resolution, ~~ice-sheet-wide record of slush ~~on~~for the GrIS, spanning nine melt seasons ~~(~~from 2016~~–~~ to 2024~~).~~. Using ~~> 300,000 S2 images and ~~a ~~supervised RF workflow in GEE~~cloud-based ML framework, we ~~show~~demonstrate that slush is widespread, climate-sensitive, and the dominant surface meltwater ~~feature~~type on the GrIS~~: it covers a mean ~2.9%~~, covering an order of ~~the ice sheet each summer and in the ~~magnitude greater area during high melt ~~year of 2019, it covered an area nine times greater ~~years than the ~~total area of other meltwater features (~~combined extent of supraglacial lakes, ~~rivers~~channels, and water~~-~~-filled crevasses~~)~~ reported in ~~other~~previous studies. Slush ~~expands inland to ~~is most extensive in the southwestern and northern basins, most persistent in the northeast and north, and reaches higher elevations ~~in warmer years and is widely concentrated over low-permeability ice slabs in the northern and western basins. Explicit representation of slush in surface mass balance, routing, and coupled hydrology–ice dynamics models is therefore necessary to capture Greenland's evolving surface hydrology and runoff. As ~~during intense melt ~~seasons lengthen and intensify, slush will ~~years, patterns that likely ~~become even more ~~reflect the distribution of bare ice, ice slabs, and firn heterogeneity across the ice sheet. Slush variability is strongly associated with firn storage capacity, meltwater supply, and air temperature, with widespread~~. Continued~~ slush development ~~of high-resolution, multi-feature supraglacial~~occurring during warm years of enhanced melt and reduced firn air content. Despite its dominance, slush remains largely absent from existing surface mass balance, hydrological, and coupled ice-dynamics modelling frameworks used to project future ice sheet behaviour; an omission that becomes increasingly consequential as the GrIS evolves under continued warming. As the GrIS warms, declining firn storage capacity, expanding ice slabs, and more frequent extreme melt events will not simply increase slush extent; they may restructure the conditions under which slush forms, persists, and refreezes. These changes may produce legacy effects that amplify future meltwater ~~datasets, which explicitly partition slush, will play a key role in~~production beyond what melt forcing alone would predict. A complete understanding ~~Greenland's future evolution~~of the GrIS response to climate change therefore requires slush to be fully represented in models alongside all other surface meltwater feature types. The nine-year, ice-sheet-wide dataset presented here provides an observational foundation for developing more physically complete representations of the evolving GrIS hydrological system.

Data availability

The slush dataset produced in this study is available from: https://doi.org/10.5281/zenodo.~~16338735~~20417415 (Glen, ~~2025~~2026). The slush delineation code used in this study ~~is available~~was adapted from~~).~~: https://doi.org/10.17863/CAM.77156 (Dell et al., 2022b). Sentinel 2 imagery is freely available via the GEE data catalogue (https://developers.google.com/earth-engine/datasets/catalog/sentinel). RACMO2.3p2 model data are available upon request from B. Noël (bnoel@uliege.be). The IMAU-FDM data are available on request from the Institute for Marine and Atmospheric Research Utrecht (imau@science.uu.nl).

Author contributions

EG, AFB and AL conceptualised the research, which was led by EG. AFB, AL, ~~KM, RD~~KEM, RLD, JM and MM contributed to the scientific content, technical details and overall structure of this paper. All co-authors contributed to the discussion of results and editing of the manuscript.

Competing interests

The authors have no competing interests to declare.

Acknowledgements

Emily Glen and Amber Leeson received support from the Natural Environment Research Council (NERC) MIIGreenland project under award NE/S011390/1 and from the European Space Agency under the POLAR+ 4DGreenland project, ESA contract no. 4000132139/20/I-EF. Alison F. Banwell received support from the U.S. National Science Foundation ~~(NSF)~~ under awards 1841607 and 2332480 to the University of Colorado Boulder (PI Banwell). Malcolm McMillan was supported by the European Space Agency POLAR+ 4DGreenland project (contract no. 4000132139/20/I-EF) and the Lancaster University~~–~~-UKCEH Centre of Excellence in Environmental Data Science. Malcolm McMillan and Jennifer Maddalena were supported by the UK NERC Centre for Polar Observation and Modelling (grant no: NE/Y006178/1).

We thank the Editor Prof. Horst Machguth, as well as Dr. Peter Tuckett and Dr. Baptise Vandecrux for their reviews, which greatly improved the quality of this manuscript. We also acknowledge the use of ChatGPT and Claude for editorial support during the revision process.

Financial support

This research has been supported by the Natural Environment Research Council (~~grant no's.~~grants NE/S011390/1 and NE/Y006178/1), the European Space Agency (grant ~~no.~~ 4000132139/20/I-EF), the National Science Foundation (~~grant no.~~grants 1841607 and 2332480).

References

Banwell, A. F., Hewitt, I., Willis, I. C., and Arnold, N.: Moulin density controls drainage development beneath the Greenland ice sheet, J. Geophys. Res. Earth Surf., 121, 2248~~–~~-2269, https://doi. org/10. 1002/2015JF003801, 2016.

Banwell, A. F., I. C. Willis, I. C., and Arnold N. S.: Modeling subglacial water routing at Paakitsoq, W Greenland, J. Geophys. Res. Earth Surf., 118, 1282~~–~~-1295, https://doi. org/10. 1002/jgrf. 20093, 2013.

Banwell, A. F., Wever, N., Dunmire, D., and Picard, G.: Quantifying Antarctic-wide ice-shelf surface melt volume using microwave and firn model data: 1980 to 2021, Geophysical Research Letters, 50, e2023GL102744~~,~~, https://doi.org/10.1029/2023GL102744, 2023.

Banwell, A. F., Arnold, N. S., Willis, I. C., Tedesco, M., and Ahlstrøm, A. P.: Modeling supraglacial water routing and lake filling on the Greenland Ice Sheet, J. Geophys. Res., 117, F04012, https://doi. org/10. 1029/2012JF002393, 2012.

Bell, R. E., Banwell, A. F., Trusel, L. D., and Kingslake, J.: Antarctic surface hydrology and impacts on ice-sheet mass balance, Nature Climate Change, 8, 1044-1052, https://doi.org/10.1038/s41558-018-0326-3, 2018.

Bonsoms, J., Oliva, M., López-Moreno, J. I., and Fettweis, X.: Rising extreme meltwater trends in Greenland Ice Sheet (1950~~–~~-2022): Surface energy balance and large-scale circulation changes. J. Clim., 37, 4851~~–~~-4866~~,~~, https://doi.org/10.1175/JCLI-D-23-0396.1, 2024.

Box, J. E. and Ski, K.: Remote sounding of Greenland supra-glacial melt lakes: Implications for subglacial hydraulics, Journal of glaciology, 53(181), 257~~–~~-264, https://doi. org/10. 3189/172756507782202883, 2007.

Brils, M., Kuipers Munneke, P., van de Berg, W. J., and van den Broeke, M.: Improved representation of the contemporary Greenland ice sheet firn layer by IMAU-FDM v1.2G, Geosci. Model Dev., 15, 7121-7138, https://doi.org/10.5194/gmd-15-7121-2022, 2022.

Breiman, L.: Random forests, Mach. Learn., 45, 5~~–~~-32~~,~~, https://doi.org/10.1023/A:1010933404324, 2001.

Chu, V. W.: Greenland ice sheet hydrology: A review, Prog. Phys. Geogr., 38, 19~~–~~-54~~,~~, https://doi.org/10.1177/0309133313507075, 2014.

Chudley, T. R., Christoffersen, P., Doyle, S. H., Dowling, T. P. F., Law, R., Schoonman, C. M., Bougamont, M., and Hubbard, B.: Controls on water storage and drainage in crevasses on the Greenland Ice Sheet, J. Geophys. Res. Earth Surf., 126, e2021JF006287~~,~~, https://doi.org/10.1029/2021JF006287, 2021.

Clerx, N., Machguth, H., Tedstone, A., and van As, D.: Modelling lateral meltwater flow and superimposed ice formation atop Greenland's near-surface ice slabs. J. Glaciol., 70, e54~~,~~, https://doi.org/10.1017/jog.2024.69, 2024.

Clerx, N., Machguth, H., Tedstone, A., Jullien, N., Wever, N., Weingartner, R., and Roessler, O.: 'In situ measurements of meltwater flow through snow and firn in the accumulation zone of the SW Greenland ice sheet', The Cryosphere, 16, 4379~~–4401.,~~-4401. https://doi.org/10.5194/tc-16-4379-2022, 2022.

Cogley, J. G., Arendt, A. A., Bauder, A., Braithwaite, R. J., Hock, R., Jansson, P., Kaser, G., Möller, M., Nicholson, L., Rasmussen, L. A., & Zemp, M. (~~2010~~2011). Glossary of glacier mass balance and related terms. IHP-VII Technical Documents in Hydrology, 86, International Hydrological Programme, UNESCO, Paris, France.

Copernicus Climate Change Service (C3S): European State of the Climate 2022, Summary, https://climate.copernicus.eu/sites/default/files/custom-uploads/ESOTC2022/PR/ESOTCsummary2022_final.pdf, last access: December 2024.

Corr, D., Leeson, A., McMillan, M., Zhang, C., and Barnes, T.: An inventory of supraglacial lakes and channels across the West Antarctic Ice Sheet, Earth Syst. Sci. Data, 14, 209~~–~~-228, https://doi. org/10. 5194/essd-14-209-2022, 2022.

Covi, F.: Processes in the percolation zone in southwest Greenland: challenges in modeling surface energy balance and melt, and the role of topography in the formation of ice slabs. PhD dissertation, University of Alaska Fairbanks, 2022. Available at: https://hdl.handle.net/11122/13116, 2022.

Culberg, R., Michaelides, R. J., & Miller, J. Z. (2024). Sentinel-1 detection of ice slabs on the Greenland ice sheet. The Cryosphere, 18(5), 2531~~–~~-2555. https://doi.org/10.5194/tc-18-2531-2024

de Fleurian, B., Werder, M. A., Beyer, S., Brinkerhoff, D. J., Delaney, I., Dow, C. F., SHMIP the subglacial hydrology model intercomparison project. Journal of Glaciology, 64(248), 897~~–916.~~,-916. https://doi.org/10.1017/jog.2018.78, 2018

Dell, R. L., Banwell, A. F., Willis, I. C., Arnold, N. S., Halberstadt, A. R. W., Chudley, T. R., and Pritchard, H. D.: Supervised classification of slush and ponded water on Antarctic ice shelves using Landsat 8 imagery, Journal of Glaciology, 68, 401~~–~~-414, 2022.

Dell, R., Banwell, A., Willis, I., Arnold, N., Halberstadt, A. R., Chudley, T., & Pritchard, H. (2022b). Supplementary Information for 'Supervised classification of slush and ponded water on Antarctic ice shelves using Landsat 8 imagery' by R.L. Dell and Others. Apollo - University of Cambridge Repository. https://doi.org/10.17863/CAM.77156

Dell, R.L., Willis, I.C., Arnold, N.S., Banwell, A., de Roda Husman, S.: Substantial contribution of slush to meltwater area across Antarctic ice shelves. Nat. Geosci. 17, 624~~–~~-630~~,~~, https://doi.org/10.1038/s41561-024-01466-6, 2024.

Dirscherl, M., Dietz, A. J., Kneisel, C., and Kuenzer, C.: Automated Mapping of Antarctic Supraglacial Lakes Using a Machine Learning Approach. Remote Sens., 12, 1203, https://doi.org/10.3390/rs12071203, 2020.

Dunmire, D., Banwell, A. F., Wever, N., Lenaerts, J. T. M., and Datta, R. T.: Contrasting regional variability of buried meltwater extent over 2 years across the Greenland Ice Sheet, The Cryosphere, 15, 2983~~–~~-3005, https://doi.org/10. 5194/tc-15-2983-2021, 2021.

Dunmire, D., Subramanian, A. C., Hossain, E., Gani, M. O., Banwell, A. F., Younas, H., and Myers, B.: Greenland Ice Sheet wide supraglacial lake evolution and dynamics: Insights from the 2018 and 2019 melt seasons, Earth and Space Science, 12, e2024EA003793~~,~~, https://doi.org/10.1029/2024EA003793, 2025.

Fan, Y., Ke, C.-Q., Luo, L., Shen, X., Livingstone, S. J., and Lea, J. M.: Expansion of supraglacial lake area, volume, and extent on the Greenland Ice Sheet from 1985 to 2023, Journal of Glaciology, 71, e4~~,~~, https://doi.org/10.1017/jog.2024.87, 2025.

Feng, S., Cook, J. M., Naegeli, K., Anesio, A. M., Benning, L. G., & Tranter, M. (2024). The impact of bare ice duration and geo-topographical factors on the darkening of the Greenland Ice Sheet. Geophysical Research Letters, 51, e2023GL104894. https://doi.org/10.1029/2023GL104894

Fettweis, X., Tedesco, M., van den Broeke, M. and Ettema, J.: Melting trends over the Greenland ice sheet (1958-2009) from spaceborne microwave data and regional climate Models, The Cryosphere, 5(2), 359-375, ISSN 19940416, doi: 10.5194/tc-5-359-2011, 2011.

Forster, R. R., Box, J. E., van den Broeke, M. R., Miège, C., Burgess, E. W., van Angelen, J. H., Lenaerts, J. T. M., Koenig, L. S., Paden, J., Lewis, C., Gogineni, S. P., Leuschen, C., and McConnell, J. R.: Extensive liquid meltwater storage in firn within the Greenland ice sheet. Nat. Geosci., 7, 95~~–~~-98~~,~~, https://doi.org/10.1038/ngeo2043, 2014.

Gantayat, P., Banwell, A. F., Leeson, A. A., Lea, J. M., Petersen, D., Gourmelen, N., and Fettweis, X.: A new model for supraglacial hydrology evolution and drainage for the Greenland Ice Sheet (SHED v1.0), Geosci. Model Dev., 16, 5803-5823, https://doi.org/10.5194/gmd-16-5803-2023, 2023.

Glen, E., Leeson, A., Banwell, A. F., Maddalena, J., Corr, D., Atkins, O., Noël, B., and McMillan, M.: A comparison of supraglacial meltwater features throughout contrasting melt seasons: southwest Greenland, The Cryosphere, 19, 1047~~–~~-1066, https://doi.org/10.5194/tc-19-1047-2025, 2025.

Glen, E. (2026). A nine-year record of slush on the Greenland Ice Sheet [Data set]. Zenodo. https://doi.org/10.5281/zenodo.20417415

Greuell, W. and Knap, W. H.: 'Remote sensing of the albedo and detection of the slush line on the Greenland ice sheet', J. Geophys. Res.-Atmos., 105, 15567~~–15576,, 2000.Halberstadt, A.R.W., Gleason, C.J., Moussavi, M.S., Pope, A., Trusel, L.D., DeConto, R.M. Antarctic Supraglacial Lake Identification Using Landsat-8 Image Classification, Remote Sens, 12, 1327, https://doi.org/10.3390/rs12081327, 2020~~-15576, https://doi.org/10.1029, 2000.

Halberstadt, A. R. W., Gleason, C. J., Moussavi, M. S., Pope, A., Trusel, L. D., and DeConto, R. M.: Antarctic Supraglacial Lake Identification Using Landsat-8 Image Classification. Remote Sens., 12, 1327, https://doi.org/10.3390/rs12081327, 2020.

Hanna E, Cappelen J, Fettweis X, Mernild, S. H., Mote, T. L., Mottram, R., Steffen, K., Ballinger, and T. J., Hall, R. J: Greenland surface air temperature changes from 1981 to 2019 and implications for ice-sheet melt and mass-balance change. Int J Climatol. 2021;41 (Suppl. 1), E1336~~–~~-E1352, https://doi.org/10.1002/joc.6771, 2021.

Hanna, E., Topál, D., Box, J. E., Buzzard, S., Christie, F. D. W., Hvidberg, C., Morlighem, M., De Santis, L., Silvano, A., Colleoni, F., Sasgen, I., Banwell, A. F., van den Broeke, M. R., DeConto, R., De Rydt, J., Goelzer, H., Gossart, A., Gudmundsson, G. H., Lindbäck, K., Miles, B., Mottram, R., Pattyn, F., Reese, R., Rignot, E., Srivastava, A., Sun, S., Toller, J., Tuckett, P. A., and Ultee, L.: Short- and long-term variability of the Antarctic and Greenland ice sheets, Nat. Rev. Earth Environ., 5, 193~~–~~-210, https://doi.org/10.1038/s43017-024-00438-8, 2024.

Hofer, S., Tedstone, A. J., Fettweis, X., and Bamber, J. L.: Decreasing cloud cover drives the recent mass loss on the Greenland Ice Sheet, Science Advances, 3, e1700584, https://doi.org/10.1126/sciadv.1700584, 2017.

Holmes, C. W.: 'Morphology and Hydrology of the Mint Julep Area, Southwest Greenland. In: Project Mint Julep Investigation of Smooth Ice Areas of the Greenland Ice Cap, 1953; Part II Special Scientific Reports.', Arctic, Desert, Tropic Information Center; Research Studies Institute; Air University, 1955.

Howat, I. M., de la Peña, S., van Angelen, J. H., Lenaerts, J. T. M., and van den Broeke, M. R.: Brief Communication ~~"Expansion~~'Expansion of meltwater lakes on the Greenland Ice ~~Sheet",~~Sheet', The Cryosphere, 7, 201~~–~~-204, https://doi. org/10. 5194/tc-7-201-2013, 2013.

Hu, J., Huang, H., Chi, Z., Cheng, X., Wei, Z., Chen, P., Xu, X., Qi, S., Xu, Y., and Zheng, Y.: Distribution and evolution of supraglacial lakes in Greenland during the 2016~~–~~-2018 melt seasons, Remote Sensing, 14, 55, 2021.

Huai, B., van den Broeke, M. R., and Reijmer, C. H.: Long-term surface energy balance of the western Greenland Ice Sheet and the role of large-scale circulation variability, The Cryosphere, 14, 4181~~–~~-4199, https://doi.org/10.5194/tc-14-4181-2020, 2020.

Humphrey, Neil F., Joel T. Harper, and Toby W. Meierbachtol:. Physical Limits to Meltwater Penetration in Firn, Journal of Glaciology 67, no. 265: 952-60. https://doi.org/10.1017/jog.2021.44, 2021.

IMBIE.: Mass balance of the Greenland Ice Sheet from 1992 to 2018, Nature, 579, 233-239, https://doi.org/10.1038/s41586-019-1855-2, 2020.

Jullien, N., Tedstone, A. J., Machguth, H., Karlsson, N. B., and Helm, V.: Greenland Ice Sheet ice slab expansion and thickening, Geophys. Res. Lett., 50, e2022GL100911~~,,~~, https://doi.org/10.1029/2022GL100911, 2023.

Jullien N, Tedstone AJ, Machguth H.: Constraining ice slab thickness at the onset of visible surface runoff from the Greenland ice sheet. Journal of Glaciology 71, e36, 1-12. https://doi.org/10.1017/jog.2025.25, 2025.

Koziol CP and Arnold N: Modelling seasonal meltwater forcing of the velocity of land-terminating margins of the Greenland Ice Sheet. Cryosphere, 12(3), 971~~–~~-991, 2018

Law R, Arnold N, Benedek C, Tedesco M, Banwell A, Willis I., 2020, Over-winter persistence of supraglacial lakes on the Greenland Ice Sheet: results and insights from a new model. Journal of Glaciology 66(257), 362-372. https://doi.org/10.1017/jog.2020.7

Leeson, A. A., Shepherd, A., Briggs, K., Howat, I., Fettweis, X., Morlighem, M., and Rignot, E.: Supraglacial lakes on the Greenland ice sheet advance inland under warming climate, Nat Clim Chang, 5, 51~~–~~-55. https://doi. org/10.1038/nclimate2463, 2015.

Leeson, A. A., Shepherd, A., Palmer, S., Sundal, A., and Fettweis, X.: Simulating the growth of supraglacial lakes at the western margin of the Greenland ice sheet, The Cryosphere, 6, 1077~~–~~-1086, https://doi. org/10. 5194/tc-6-1077-2012, 2012.

Liang, Y.-L., Colgan, W., Lv, Q., Steffen, K., Abdalati, W., Stroeve, J., Gallaher, D., and Bayou, N.: A decadal investigation of supraglacial lakes in West Greenland using a fully automatic detection and tracking algorithm, Remote Sensing of Environment, 123, 127~~–~~-138, https://doi.org/10.1016/j.rse.2012.03.020, 2012.

Lüthje, M., Pedersen, L. T., Reeh, N., and Greuell, W.: Modelling the evolution of supraglacial lakes on the West Greenland ice-sheet margin, J. Glaciol., 52, 608~~–~~-618, https://doi.org/10. 3189/172756506781828386, 2006.

Machguth, H., MacFerrin, M., van As, D., Box, J. E., Charalampidis, C., Colgan, W., Fausto, R, S., Meijer, H. A. J., Mosley-Thompson., and van de Wal, R. S. W.: Greenland meltwater storage in firn limited by near-surface ice formation. Nature Clim Change 6, 390~~–~~-393, https://doi. org/10. 1038/nclimate2899, 2016.

Machguth, H., Tedstone, A., and Mattea, E.: Daily variations in Western Greenland slush limits, 2000~~–~~-2021, Journal of Glaciology, 69(273), 191-203, https://doi.org/10.1017/jog.2022.65, ~~2023~~2022.

McFeeters, S. K.: The use of the Normalized Difference Water Index (NDWI) in the delineation of open water features', International Journal of Remote Sensing, 17(7), 1425~~–1432,~~,-1432, https://doi.org/10.1080/01431169608948714., 1996.

Melling, L., Leeson, A., McMillan, M., Maddalena, J., Bowling, J., Glen, E., Sandberg Sørensen, L., Winstrup, M., and Lørup Arildsen, R.: Evaluation of satellite methods for estimating supraglacial lake depth in southwest Greenland, The Cryosphere, 18, 543-558, https://doi.org/10.5194/tc-18-543-2024, 2024.

Miège, C., Forster, R. R., Brucker, L., Koenig, L. S., Solomon, D. K., Paden, J. D., Box, J. E., Burgess, E. W., Miller, J. Z., McNerney, L., and Brautigam, N.: Spatial extent and temporal variability of Greenland firn aquifers detected by ground and airborne radars, J. Geophys. Res. Earth Surf., 121, 2381~~–~~-2398~~,~~, https://doi.org/10.1002/2016JF003869, 2016.

Mikkelsen, A. B., Hubbard, A., MacFerrin, M., Box, J. E., Doyle, S. H., Fitzpatrick, A., Hasholt, B., Bailey, H. L., Lindbäck, K., and Pettersson, R.: Extraordinary runoff from the Greenland ice sheet in 2012 amplified by hypsometry and depleted firn retention, The Cryosphere, 10, 1147~~–~~-1159, https://doi.org/10.5194/tc-10-1147-2016, 2016.

Miles K. E., Willis I. C., Benedek, C. L., Williamson, A. G., and Tedesco, M.: Toward Monitoring Surface and Subsurface Lakes on the Greenland Ice Sheet Using Sentinel-1 SAR and Landsat-8 OLI Imagery, Front. Earth Sci. 5:58, https://doi.org/10.3389/feart.2017.00058, 2017.

Moon, T., Mankoff, K., Fausto, R., Fettweis, X., Loomis, B., Mote, T., et al.: Arctic Report Card 2022: Greenland Ice Sheet, NOAA Technical Report OAR ARC 22-05~~,~~, https://doi.org/10.25923/c430-hb50, 2022.

Mottram, R., Hansen, N., Hogg, A. E., Rodehacke, C. B., Simonsen, S. B., and Wallis, B. J.: The Greenlandification of Antarctica, Nature Geoscience, 18, 928-930, https://doi.org/10.1038/s41561-025-01805-1 , 2025.

Moussavi, M., Pope, A., Halberstadt, A. R. W., Trusel, L. D., Cioffi, L., and Abdalati, W.: Antarctic supraglacial lake detection using Landsat 8 and Sentinel-2 imagery: Towards continental generation of lake volumes. Remote Sens., 12(1), 134~~,~~, https://doi.org/10.3390/rs12010134, 2020.

Nowicki, S., Goelzer, H., Seroussi, H., Payne, A. J., Lipscomb, W. H., Abe-Ouchi, A., Agosta, C., Alexander, P., Asay-Davis, X. S., Barthel, A., Bracegirdle, T. J., Cullather, R., Felikson, D., Fettweis, X., Gregory, J. M., Hattermann, T., Jourdain, N. C., Kuipers Munneke, P., Larour, E., Little, C. M., Morlighem, M., Nias, I., Shepherd, A., Simon, E., Slater, D., Smith, R. S., Straneo, F., Trusel, L. D., van den Broeke, M. R., and van de Wal, R.: Experimental protocol for sea level projections from ISMIP6 stand-alone ice sheet models, The Cryosphere, 14, 2331-2368, https://doi.org/10.5194/tc-14-2331-2020, 2020.

Noël, B., van de Berg, W. J., Lhermitte, S., and van den Broeke, M. R.: Rapid ablation zone expansion amplifies North Greenland mass loss. Science Advances, 5(9), 2~~–~~-11. https://doi.org/10.1126/sciadv.aaw0123, 2019.

Otosaka, I. N., Shepherd, A., Ivins, E. R., Schlegel, N.-J., Amory, C., van den Broeke, M. R., Horwath, M., Joughin, I., King, M. D., Krinner, G., Nowicki, S., Payne, A. J., Rignot, E., Scambos, T., Simon, K. M., Smith, B. E., Sørensen, L. S., Velicogna, I., Whitehouse, P. L., A, G., Agosta, C., Ahlstrøm, A. P., Blazquez, A., Colgan, W., Engdahl, M. E., Fettweis, X., Forsberg, R., Gallée, H., Gardner, A., Gilbert, L., Gourmelen, N., Groh, A., Gunter, B. C., Harig, C., Helm, V., Khan, S. A., Kittel, C., Konrad, H., Langen, P. L., Lecavalier, B. S., Liang, C.-C., Loomis, B. D., McMillan, M., Melini, D., Mernild, S. H., Mottram, R., Mouginot, J., Nilsson, J., Noël, B., Pattle, M. E., Peltier, W. R., Pie, N., Roca, M., Sasgen, I., Save, H. V., Seo, K.-W., Scheuchl, B., Schrama, E. J. O., Schröder, L., Simonsen, S. B., Slater, T., Spada, G., Sutterley, T. C., Vishwakarma, B. D., van Wessem, J. M., Wiese, D., van der Wal, W., and Wouters, B.: Mass balance of the Greenland and Antarctic ice sheets from 1992 to 2020, Earth Syst. Sci. Data, 15, 1597~~–~~-1616, https://doi.org/10.5194/essd-15-1597-2023, 2023.

Otto J, Holmes, F. A. and Kirchner, N.: Supraglacial lake expansion, intensified lake drainage frequency, and first observation of coupled lake drainage, during 1985~~–~~-2020 at Ryder Glacier, Northern Greenland, Front. Earth Sci.,10:978137, https://doi.org/10.3389/feart.2022.978137, 2022.

Porter, C., Morin, P., Howat, I., Noh, M.-J., Bates, B., Peterman, K., Keesey, S., Schlenk, M., Gardiner, J., Tomko, K.,Willis, M., Kelleher, C., Cloutier, M., Husby, E., Foga, S.,Nakamura, H., Platson, M., Wethington, M. Jr., Williamson,C., Bauer, G., Enos, J., Arnold, G., Kramer, W., Becker, P.,Doshi, A., D'Souza, C., Cummens, P., Laurier, F., and Bo-jesen, M.: ArcticDEM, v3.0, Harvard Dataverse [data set], https://doi.org/10.7910/DVN/OHHUKH, 2023 [Date Accessed: April 2024].

Qayyum, N., Ghuffar, S., Ahmad, H., Yousaf, A., and Shahid, I.: Glacial Lakes Mapping Using Multi Satellite PlanetScope Imagery and Deep Learning. ISPRS Int. J. Geo-Inf., 9, 560, https://doi.org/10.3390/ijgi9100560, 2020.

Rawlins, L. D., Rippin, D. M., Sole, A. J., Livingstone, S. J., and Yang, K.: Seasonal evolution of the supraglacial drainage network at Humboldt Glacier, North Greenland, between 2016 and 2020, The Cryosphere Discuss., https://doi. org/10. 5194/tc-2023-23, 2023.

Rippin, D. and Rawlins, L.: Supraglacial River Networks, In International Encyclopedia of Geography, edited by: Richardson, D., Castree, N., Goodchild, M. F., Kobayashi, A., Liu, W., and Marston, R. A., https://doi.org/10.1002/9781118786352.wbieg2072, 2021

Ryan, J. C., Smith, L. C., van As, D., Cooley, S. W., Cooper, M. G., Pitcher, L. H., and Hubbard, A.: Greenland Ice Sheet surface melt amplified by snowline migration and bare ice exposure. Sci. Adv., 5, eaav3738, https://doi.org/10.1126/sciadv.aav3738, 2019.

Ryan, J.C., Cooper, M.G., Cooley, S.W. *et al.* Meltwater ponding has an underestimated radiative effect on the surface of the Greenland Ice Sheet. *Nat Commun* **16**, 8274, ~~,~~https://doi.org/10.1038/s41467-025-62503-5, 2025

Sasgen, I., Wouters, B., Gardner, A. S., King, M. D., Tedesco, M., Landerer, F. W., Dahle, C., Save, H., and Fettweis, X.: Return to rapid ice loss in Greenland and record loss in 2019 detected by the GRACE-FO satellites, Communications Earth & Environment, 1, 8, https://doi.org/10.1038/s43247-020-0001-2, 2020.

Selmes, N., Murray, T., and James T. D.: Fast draining lakes on the Greenland ice sheet. Geophys Res Lett, 38, L15501, https://doi. org/10. 1029/2011GL047872, 2011.

Slater, T., Shepherd, A., McMillan, M. Leeson, A., Gilbert, L., Muir, A., Kuipers Munneke, P., Noel, B., Fettweis, X., van den Broeke, M., Briggs, K.: Increased variability in Greenland Ice Sheet runoff from satellite observations. Nat Commun 12, 6069~~,~~, https://doi.org/10.1038/s41467-021-26229-4, 2021

Stokes, C. R., Sanderson, J. E., Miles, B. W. J., Jamieson, S. S. R., and Leeson, A. A.: Widespread distribution of supraglacial lakes around the margin of the East Antarctic Ice Sheet, Scientific Reports, 9, 13823, https://doi.org/10.1038/s41598-019-50343-5, 2019.

Sundal, A. V., Shepherd, A., Nienow, P., Hanna, E., Palmer, S., and Huybrechts, P.: Evolution of supra-glacial lakes across the Greenland ice sheet, Remote Sens. Environ., 113(10), 2164~~–~~-2171, https://doi.org/10.1016/j.rse.2009.05.018, 2009.

Tedesco, M. and Fettweis, X.: Unprecedented atmospheric conditions (1948~~–~~-2019) drive the 2019 exceptional melting season over the Greenland ice sheet, The Cryosphere, 14, 1209-1223, https://doi.org/10.5194/tc-14-1209-2020, 2020.

Tedesco, M., Willis, I. C., Hoffman, M. J., Banwell, A. F., Alexander, P., and Arnold, N. S.: Ice dynamic response to two modes of surface lake drainage on the Greenland Ice Sheet, Environmental Research Letters, 8, 034007~~.~~, https://doi.org/10.1088/1748-9326/8/3/034007, 2013

Tedstone, A. and Machguth, H.: Increasing surface runoff from Greenland's firn areas, Nature Climate Change 12, 672~~–~~-676, https://doi.org/10.1038/s41558-022-01371-z, 2022.

Tedstone, A. J., Bamber, J. L., Cook, J. M., Williamson, C. J., Fettweis, X., Hodson, A. J., and Tranter, M.: Dark ice dynamics of the south-west Greenland Ice Sheet, The Cryosphere, 11, 2491~~–~~-2506, https://doi.org/10.5194/tc-11-2491-2017, 2017.

Tedstone, A., Machguth, H., Clerx, N. *et al.* Concurrent superimposed ice formation and meltwater runoff on Greenland's ice slabs. *Nat Commun* **16**, 4494 (2025~~).~~). https://doi.org/10.1038/s41467-025-59237-9

The Firn Symposium team: Firn on ice sheets, Nature Reviews Earth & Environment, 5, 79-99, https://doi.org/10.1038/s43017-023-00507-9, 2024.

Trusel, L. D., Das, S. B., Osman, M. B., Evans, M. J., Smith, B. E., Fettweis, X., McConnell, J. R., Noël, B. P. Y., and Broeke, M. R. van den: Nonlinear rise in Greenland runoff in response to post-industrial Arctic warming, Nature, 564, 104~~–~~-108, 2018 https://doi.org/10.1038/s41586-018-0752-4, 2018.

Tuckett, P. A., Sole, A. J., Livingstone, S. J., Jones, J. M., Lea, J. M., and Gilbert, E.: Continent-wide mapping shows increasing sensitivity of East Antarctica to meltwater ponding, Nature Climate Change, 15, 775-783, 2025.

van As, D., Bech Mikkelsen, A., Holtegaard Nielsen, M., Box, J. E., Claesson Liljedahl, L., Lindbäck, K., Pitcher, L., and Hasholt, B.: Hypsometric amplification and routing moderation of Greenland ice sheet meltwater release, The Cryosphere, 11, 1371~~–~~-1386, https://doi.org/10.5194/tc-11-1371-2017, 2017.

van den Broeke, M. R., Kuipers Munneke, P., Noël, B., Reijmer, C., Smeets, P., van de Berg, W. J., et al.: Contrasting current and future surface melt rates on the ice sheets of Greenland and Antarctica: Lessons from in situ observations and climate models, PLOS Climate, 2, e0000203, https://doi.org/10.1371/journal.pclm.0000203, 2023.

Vandecrux, B., MacFerrin, M., Machguth, H., Colgan, W. T., van As, D., Heilig, A., Stevens, C. M., Charalampidis, C., Fausto, R. S., Morris, E. M., Mosley-Thompson, E., Koenig, L., Montgomery, L. N., Miège, C., Simonsen, S. B., Ingeman-Nielsen, T., and Box, J. E.: Firn data compilation reveals widespread decrease of firn air content in western Greenland, The Cryosphere, 13, 845~~–~~-859, https://doi.org/10.5194/tc-13-845-2019, 2019.

Williamson, A. G., Banwell, A. F., Willis, I. C., and Arnold, N. S.: Dual-satellite (Sentinel-2 and Landsat 8) remote sensing of supraglacial lakes in Greenland, The Cryosphere, 12, 3045~~–~~-3065, https://doi.org/10.5194/tc-12-3045-2018, 2018.

Williamson, A. G., Arnold, N., Banwell, A., and Willis, I.: A Fully Automated Supraglacial lake area and volume Tracking ~~(“FAST”)~~('FAST') algorithm: Development and application using MODIS imagery of West Greenland, Remote Sens. Environ., 196, 113~~–~~-133, https://doi.org/10.1016/j.rse.2017.04.032, 2017.

Yang, K., Smith, L. C., Sole, A., Livingstone, S. J., Cheng, X., Chen, Z., and Li, M.: Supraglacial rivers on the northwest Greenland Ice Sheet, Devon Ice Cap, and Barnes Ice Cap mapped using Sentinel-2 imagery, Int. J. Appl. Earth Obs., 78, 1~~–~~-13, https://doi.org/10.1016/j.jag.2019.01.008, 2019.

Zhang, W., Yang, K., Smith, L. C., Wang, Y., van As, D., Noël, B., Lu, Y., Liu, J.: Pan-Greenland mapping of supraglacial rivers, lakes, and water-filled crevasses in a cool summer (2018) and a warm summer (2019), Remote Sensing of Environment, 297, 113781~~,, 2023.~~, https://doi.org/10.1016/j.rse.2023.113781, 2023.